POLYTECHNIC UNIVERSITY OF BUCHAREST
Şcoala doctorală de Inginerie Industrială şi Robotică

PhD Thesis Summary

Research on optimisation of the functional behavior of high speed main spindle assemblies with bearings

Author, Ing. Andrei GHEORGHIȚĂ

PhD supervisor, Prof. dr. ing. George CONSTANTIN

Bucharest, 2021

FOREWORD

Optimizing the functional behaviour of main shaft assemblies with high speed bearings is the subject of important research in the field of mechanics in general and machine tools in particular.

At the same time, the subject of the thesis was a challenge at the level of knowledge of the phenomena involved in the operation of the main shaft assembly for high speeds supported on bearings, but also in terms of treating such an assembly in terms of experimental research and complex modelling. with various types of models that can capture aspects related to the influence of various constructive and functional parameters, reaching optimization solutions. From this point of view, going through the research stages was a unique school and a special experience of transforming the doctoral student into a researcher characterized by the desire for knowledge, the search for new solutions, clarity and scientific rigor.

The research and elaboration of the doctoral thesis took place under the rigorous guidance of the scientific coordinator, prof. Univ. Dr. Eng. George Constantin, to whom I extend my full gratitude and sincere thanks for the competent guidance, help, kindness and availability granted during the doctoral school, as well as for the completion and writing of the doctoral thesis.

At the same time, I express my sincere thanks to the Polytechnic University of Bucharest, the Faculty of Industrial and Robotic Engineering and the Department of Robots and Production Systems for supporting all doctoral studies, for the facilities provided, as well as for permanent advice and effective support in research. .

I would like to extend my warmest thanks to all those who have left their scientific mark on the road to conducting research, starting with the admission to the doctorate and until the completion of the thesis. Among them I gratefully mention the members of the Steering Committee, who analyzed step by step the evolution of research and who expressed observations and suggestions particularly useful for guiding and improving the content of scientific reports and thesis - prof. Univ. emeritus Dr. Eng. Adrian Ghionea, univ. prof. dr. eng. Miron Zapciu and prof. univ. dr. eng. Tiberiu Dobrescu. For the collaboration and support in various stages of the research, experimental or modeling and simulation and for the collaboration in the dissemination of the results I gratefully mention prof. Univ. dr. eng. Constantin Dogariu and associate professor dr. eng. Claudiu Florinel Bîșu.

Last but not least, I would like to thank my family, colleagues and friends for their understanding and support throughout the elaboration of the research and the thesis.

CONTENT

CHAPTER 1
INTRODUCTORY NOTIONS ON MAIN SHAFTS FOR HIGH SPEEDS AND THE OBJECTIVES OF THE DOCTORAL THESIS

1.1. INTRODUCTION

The mechanical assembly of the main shaft-housing type with bearings is one of the most important parts of a machine tool, because the precision of machining the parts is directly influenced by the operation of the assembly in optimal parameters. Dynamic, thermal behaviour and vibration analysis of shafts are the subject of important research in the field of mechanics in general and machine tools in particular ([192], [189], [1], [10], [17], [25], [55], [109], [163], [191], [166], [167], [168], [47]).

High-speed, application-specific assemblies are sophisticated, delicate and expensive. The ability of the shafts to operate at high speeds is determined by the dynamic characteristics of the support bearings [36]. The higher the rotation speed, the smaller the size of the bearings and the shaft must be. Machine tools are becoming more and more demanding, with higher performance and the widest possible use, but in conditions of smooth operation (without vibrations) and with minimal heat release.

Noise and vibration occur during the operation of the main shaft, which results in unstable cutting, improper surface finishing and possible damage to parts, tools or shafts. Thermal expansion and vibration during the cutting operation can be a problem, especially for applications that require precision machining.

Heat and vibration problems significantly affect the properties of shafts, such as: rigidity, lifespan, accuracy. Modeling, simulation and optimization of the operation of the main shaft-housing with bearings assemblies with regard to the above-mentioned aspects continue to be researched with interest in the literature.

1.2 OBJECTIVES OF THE DOCTORAL THESIS

In the research activity will be considered as study models, both assemblies of main shaft-housing with bearings with the transmission of motion from the motor by transmission through belts, and main shafts integrated with the electric motor. In Figs. 1.4. the main and secondary

objectives, specific to the research objectives carried out within the doctoral thesis, are represented schematically

MAJOR OBJECTIVES OF THE RESEARCH	SECONDARY OBJECTIVES OF THE RESEARCH
MO1. Objectives regarding the need and substantiation of the field of study	
MO2. Review of the literature with reference to the researched topic	**SO2.1** Complex analysis of the preload distribution in a group of angular contact bearings
	SO 2.2 Analysis of heat phenomena in main shafts of high speeds with bearings and transmission of movement through belts
	SO 2.3 Analysis of thermal phenomena in main shafts of high speeds operated from the outside and with integrated AC electric motor
MO3. Theoretical contributions regarding the achievement of mathematical / CAD / numerical models regarding the technical system / studied process	**SO 3.1** Calculation of thermal deformation at the level of the main shaft-bearings assembly with predefined geometry and possible implications on operation
	SO 3.2 Models of the main shaft with bearings using thermal networks with different degrees of complexity
	SO 3.3 Evolutionary algorithms for complex problems with hard-to-find solutions, such as the calculation of the contact angle for angular contact ball bearings, an essential variable for the calculation of the heat generated by the bearing
	SO 3.4 Proposals for improved techniques for generating the thermal network that models the transmission of heat through shafts with bearings generated by the bearing
	SO 3.5 Temperature-frequency dependence analysis for a shaft-bearing assembly
	SO 3.6 Complex thermomechanical analysis of externally driven main shafts - Inventor Professional and SolidWorks finite element modeling and simulation and SolidWorks multiphysics
	SO 3.7 Transient thermomechanical analysis of externally driven main shafts (SolidWorks).
	SO 3.8 Optimization of the durability of angular contact ball bearings according to the working parameters of the main shaft
MO4. Original application contributions on numerical simulations on models	
MO5. Original contributions on experimental research made on the functional model	
MO6. Discussions and conclusions	

Fig.1.1. Major objectives (MO) and secondary objectives (SO) of the doctoral the

CHAPTER 2
ANALYSIS ON THE CURRENT STATE DYNAMIC BEHAVIOR OF SPINDLE BEARINGS AND FUNCTIONAL OPTIMIZATION ANDTHEIR ISSUES

2.1. ANALYSIS OF THE SHAFT-BEARING ASSEMBLY BY THE FINITE ELEMENT METHOD

In the analysis of the dynamic regime of rotating shaft, two important methods are outlined: the transfer matrix method (MMT) and the finite element method (MEF). MMT is a discretization principle and can be used to determine natural frequencies, and modal analysis [155] . The method consists in defining the boundary conditions (on the border) at one end and updating the system information with each shaft segment, up to the other end. The information can be: state, displacement, slope, moment or shear force at each limit of the segment section. The information is transferred from one section to another until the transfer matrix is calculated over the entire system. MMT can be applied to any linear system and the method can be demonstrated using a system of masses connected by springs between them, subjected to an end force.

2.2. ANALYSIS OF THE STATIC BEHAVIOR OF HIGH SPEED SHAFTS - DISPLACEMENTS AND DEFORMATIONS - USING MEF

The mathematical models of extended rotor beams correspond to the three theories: Euler-Bernouli, Rayleigh and Timoshenko F_h [79]. Euler-Bernouli theory considers translational inertia, Rayleigh also considers relational inertia and Timoshenko also considers the deformation produced by shear. From this point of view, at present the most complete model is the one based on Timoshenko's theory.

There are two methods for developing the equations for beams and further for shafts: 1.The direct method using the laws of elastic deformation mechanics 2.Variational calculus - the method of potential energy (minimum potential energy), one of the methods of variational calculus. In Timoshenko's theory, the plane of the section no longer remains perpendicular to the neutral axis of the section. The shear force is included in the rotation with the angle β of the beam. The total deformation of the beam at the point $\hat{x}$ is now composed of two parts, one corresponding to bending ($\hat{\phi}$) and another caused by shearing ($\hat{\beta}$) (Fig. 2.5).

$$\frac{d\hat{v}}{d\hat{x}} = \hat{\phi}(\hat{x}) + \beta(\hat{x}). \tag{2.1}$$

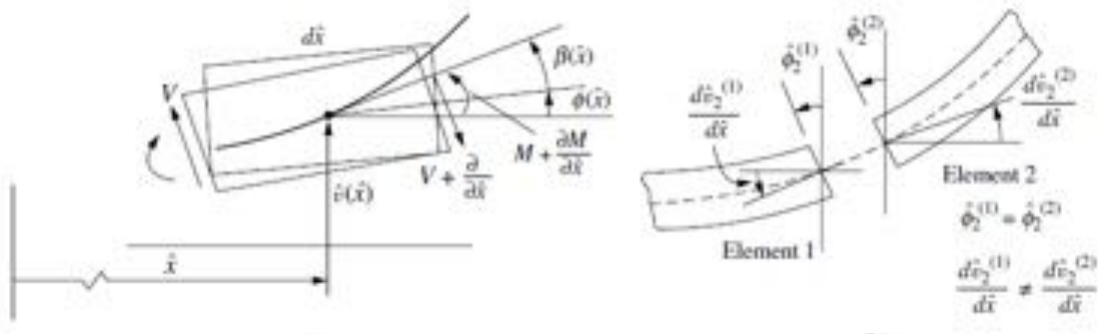

a b

Fig. 2.5. Total deformation of the beam: a - Timoshenko element;
b - two sections with meeting point in node 2

2.3. VIBRATION ANALYSIS FOR HIGH SPEED SHAFTS

Bearing manufacturing technology is very advanced today. However, it often happens that vibration in shaft with bearings to occur naturally. These situations do not reduce the performance of the bearings and are accepted as normal phenomena of bearings unless defects occur. Bearing vibrations, in response to the action of one or more forces acting on them, are usually studied using modal analysis, in the context of rotating systems, such as the main shaft with bearings. The system's natural frequencies are most often analyzed as a system frequency response - FRF (Frequency Response Function) to an excitation force.

The critical shaft speed can be defined as a rotational speed in which the vibration amplitude has a maximum (as a function of the rotational speed). Mechanical spatial models can be represented in matrix form (the case of shaft with bearings) in the form:

$$[M]\{\ddot{q}(t)\} + [C]\{\dot{q}(t)\} + [K]\{q(t)\} = \{F(t)\}, \tag{2.41}$$

where [M] is the mass, [C] - damping, [K] - stiffness, {F (t)} - the excitation force, and q (t) - the system response. The modal analysis aims at two calculation directions: natural frequencies (frequencies at which the system oscillates without the intervention of external force - excitation or damping) and FRF. When the forced frequency is equal to that of the system, the resonance phenomenon occurs and the amplitude of the signal increases several times, a harmful phenomenon, which in the case of the main shaft-bearings can lead to malfunction or even destruction.

2.4. MULTIBODY SYSTEMS AND ANALYSIS OF THE POSSIBILITY OF APPLICATION TO THE SHAFT-BEARING ASSEMBLY

Multibody systems are associated with the study of the dynamic behavior of interconnected rigid or flexible bodies (fig. 2.9), each of which can have large translational and rotational displacements. A multibody system is a system consisting of several bodies interconnected by kinematic connections that limit the relative motion of the bodies they connect.

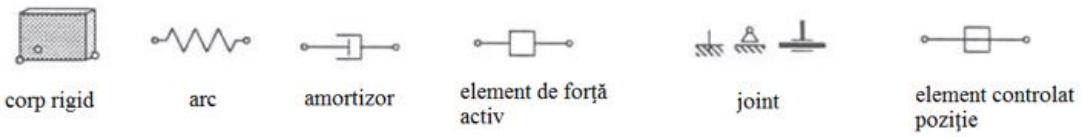

Fig. 2.9. Elements of a multibody system

The equations of motion describe the dynamic behavior of a multibody system. These can be obtained by a number of methods: Newton-Euler equations, Lagrange equations (extension of D'Alembert's principle) and Kane's equations using the principle of virtual mechanical work [110] etc.

$$M(q)\ddot{q} - Q_v + C_q^T \lambda = F, \tag{2.51}$$

$$C(q,\dot{q}) = 0, \tag{2.52}$$

where q - generalized coordinates, M (q) –mass matrix, C - constraints, Cq - Jacobian of constraints (derivatives)λ – Lagrange multipliers of constraints, Qv - Coriolis force and centrifugal force (quadratic velocity vector).

2.5. CALCULATION OF THE CONTACT ANGLE FOR BEARINGS WITH ANGLE CONTACT BALLS

$$\alpha(i+1) = \alpha(i) + \frac{\frac{F_a}{ZD^2K} - \sin\alpha\left(\frac{\cos\alpha^0}{\cos\alpha} - 1\right)^{1.5}}{\cos\alpha\left(\frac{\cos\alpha^0}{\cos\alpha} - 1\right)^{1.5} + 1.5\tan\left(\frac{\cos\alpha^0}{\cos\alpha} - 1\right)^{0.5}\cos\alpha^0}. \tag{2.55}$$

In formula (2.55) K (displacement constant) is a function of curvature and is taken from the graph or tables [104]. In dynamic mode, however, the values of the angles for each ball must be considered (Fig. 2.10).

To find these angles, the method of the minimum of a nonlinear fmincon system in Matlab, the minimum of a function of several variables with constraints, is used. The equations used are [79]:

$$A_{1j} = BD\sin\alpha^0 + \delta_a + \theta\Re_i\cos\psi_j, \tag{2.56}$$

$$A_{2j} = BD\sin\alpha^0 + \delta_r\cos\psi_j, \tag{2.57}$$

$$\cos\alpha_{oj} = \frac{X_{2j}}{(f_0 - 0.5)D + \delta_{oj}}, \tag{2.58}$$

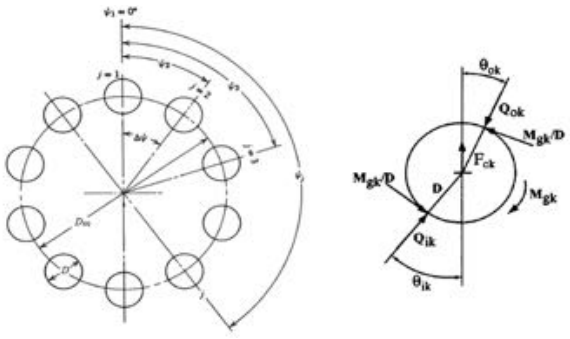

a b

Fig. 2.10. Ball bearing model: a - ball positions in the radial plane yz (x is the bearing axis);

2.6. CALCULATION OF HEAT GENERATED BY ANGLE CONTACT BALL BEARINGS AND CYLINDRICAL ROLLER BEARINGS

In the calculation of the heat produced by the bearings, calculations related to forces acting in a dynamic regime on the bearing ball and calculations related to the bearing geometry are involved. In shafts with high speed bearings with transmission of motion through the belts, there are two major sources of heat: the heat generated in the cutting process and the heat generated by the bearings. If the main shaft is integrated with the electric motor, the electric motor will generate an additional heat source through the stator.

The heat generated by the bearings in dynamic mode will be treated in the following. The following sources of friction are considered:

- running elastic hysteresis;
- sliding of the rolling element on the ring produced by the geometry of the surfaces;
- slipping caused by deformation of contact elements;
- viscosity of the lubricant;
- rubbing the elements of the cage.

There are three main modes of heat transfer between masses with different temperatures: conduction through solid structures, convection of heat from solid structures to moving fluids, and heat radiation between masses separated by spaces.

2.7. ANALYSIS OF THE THERMAL REGIME OF THE MAIN BEARINGS

A thermal network is defined as a set of nodes and conductors (resistors) being similar to an electrical circuit, therefore laws similar to Kirchoff's laws can be applied to solve problems in the case of thermal networks with heat sources (Fig. 2.13) [68].

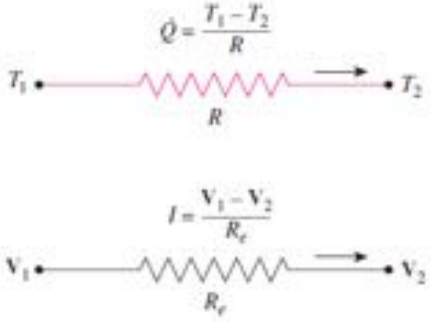

Fig. 2.13. Similarity thermal network-electrical network

Due to the discontinuities of the main shaft-bearing structure that includes balls (and / or rollers), rings, main shaft and housing, it is difficult (or practically impossible) to find an analytical formula for calculating the temperature at each point for the entire structure [79]. The center of each element is described as the location of a mediated temperature, the whole element having the same temperature (Fig. 2.15). The heat from the center of an element is transferred to the centers of adjacent elements through the contact areas (areas). The equation of each node is calculated with finite differences (Fig. 2.16) ([183], [23], [88], [19], [107]):

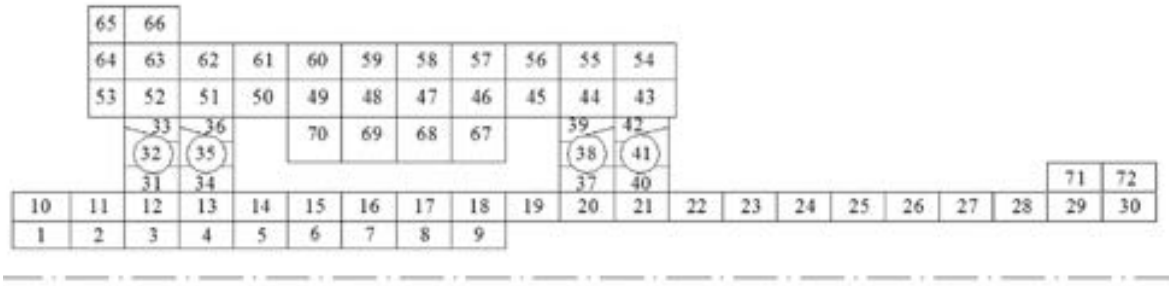

Fig. 2.15. Discretization of a main shaft-bearing bearing assembly (adaptation after [183])

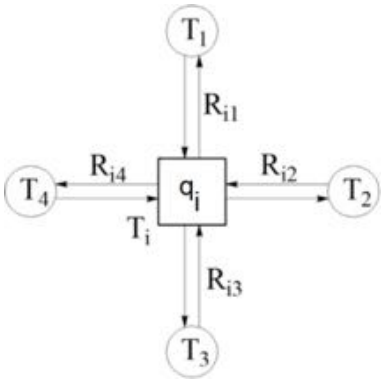

Fig. 2.16. Temperature in the node and in the nodes adjacent to node i

2.8. OPTIMIZING THE FUNCTIONAL BEHAVIOR OF MAIN SHAFT-BEARING ASSEMBLIES

Functional optimization of trees for high speeds in dynamic mode is generally a difficult subject, the algorithms used for optimization being very varied, including neural network techniques and evolutionary algorithms. Optimizations take into account several parameters (multi-parameter optimization) that influence a process characterized by the process performance criterion. Most works consider a single criterion, for example, temperature at certain points, maximum temperature at certain points, bearing lubrication, bearing durability, pumping power and friction loss in the pumped liquid, minimization based on an optimum of the function graph mathematics that describes these relationships. Evolutionary algorithms have been proposed as an optimization tool in applications that use especially sliding bearings. Genetic algorithms as part of evolutionary techniques are used in optimization problems that may also have areas of discontinuity. This property is required for use in the functional optimization of bearing shafts.

CHAPTER 3
ANALYSIS AND OPTIMIZATION OF THE THERMAL REGIME OF THE MAIN SHAFTS WITH BEARINGS

3.1. DISTRIBUTION OF LOAD TO A CONSTRUCTION OF (M, N) BEARING BEARINGS WITH ANGLE CONTACT

Dynamic contact angle values for angular contact bearings are important for durability but also for reducing the power consumed by the shaft. Various combinations of axial radial ball bearings with angular contact are widely used to improve the ability to absorb cutting forces. It is known that preload and stiffness are mutually influenced, there is a directly proportional relationship between the two sizes [114]. As a result, calculations for bearing combinations can be performed taking into account the load-strain torque for each bearing [211].

3.2 HEAT GENERATION PHENOMENA IN ALTERNATING CURRENT ELECTRIC MOTORS INTEGRATED WITH HIGH SPEED SHAFTS - THEORETICAL AND NUMERICAL RESULTS

The analysis of the behavior of the main shafts supported on bearings from the point of view of deformations, displacements, temperature and vibrations is made for two distinct types of assemblies: a) with transmission of motion from an external motor by specific mechanisms (belt drive, gear); b) with motor integrated with the main shaft.

Both situations have advantages and disadvantages, the thermal analysis in the second case being more complicated and complex because the electric motor with which this type of shaft is usually equipped generates additional heat sources in the stator and rotor windings, entering the equation of thermal balance. In figure 3.4, the typical scheme for an AC motor integrated with the main shaft with bearings is presented.

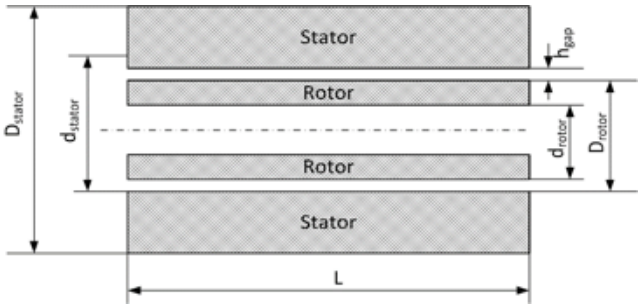

Fig. 3.4 Geometry of AC motor components (adapted from [18])

Typically, main shafts have an alternating current (AC) motor integrated with continuously adjustable speed [41]..

Motor losses can be divided into two categories: mechanical losses and electrical losses. Mechanical losses are caused by friction in the bearings and the flow of air around the components mounted on the main shaft.. Electrical losses are caused by losses from copper windings in the primary circuit (P_{pc}), iron - Pir, hysteresis - P_h and leakage phenomena - P_e losses from copper windings in the secondary, (P_{sc}) losses caused by leakage of current induced in stator and rotor including outside the motor - P_{str} (including gaps in the rotor-stator-housing spaces) and electromagnetic friction - P_{fw} [106]. We note the mechanical power at the output P_{m_out} and the electrical power at the input P_{el_in}. The balance of power leads to the equation:

$$P_{el\_in} = P_{m\_out} + P_{pc} + P_{ir} + P_{sc} + P_{str} + P_{fw}, \tag{3.16}$$

$$P_{m\_out} = T_t \cdot \omega_{rotor}. \tag{3.17}$$

where T_t represents the torque of the tool holder and ω_{rotor} is the angular velocity of the cutting tool. When $P_{m\_out} = 0$, the equation (3.2) has a simplified form:

$$P_{el\_in} = P_{pc} + P_{ir} + P_{sc} + P_{str} + P_{fw}. \tag{3.18}$$

Measured values are considered for $R_1 = 0.05\ \Omega$ and for R_2 values of the same order of magnitude, at a constant line current of 18 A when idling - no load. Rotor core iron losses are combinations of magnetic hysteresis (the term containing the K_H constant) and very small current leaks (the term containing the K_E constant) and are described as frequency functions in 1], starting from a Steinmetz model of losses in the iron core described by:

$$P_{ir} = K_H \cdot f + K_E \cdot f^2. \tag{3.21}$$

$$K_H = 3 \cdot K_E \cdot f_{\text{nominal}}, \tag{3.22}$$

$$P_{ir} = 3 \cdot K_E \cdot f_{\text{nominal}} \cdot f + K_E \cdot f^2 = K_E \cdot f \cdot (3 \cdot f_{\text{nominal}} + f). \tag{3.23}$$

For an AC electric motor, the n_{sync} (rpm) synchronization frequency is given by $n_{sync} = 2f / p$ where f represents the frequency of the power supplier (in the current study $f = 50$ Hz) and p the number of poles (in the current study $p = 4$). As a result, for a three-phase motor:

$$N_{\text{sync}} = \frac{2f}{p} \cdot \left(\frac{60 \quad \text{secunde}}{\text{minut}} \right) = \frac{120f}{4} = 1500 \text{ rpm}. \tag{3.24}$$

The charts represented by frequency poles vs. the rotational speeds of the rotor are linear, due to a test motor with a maximum speed of $n_{\max} = 25\,000$ rpm, we can write:

$$f_{\text{nominal}} = (N_{\max} \times f) / n_{\text{sync}} = (25000 \times 50)/1500 \approx 833 \text{ Hz}. \tag{3.25}$$

The nominal parameters K_H and K_E are determined experimentally for each type of

motor and, as a result, this aspect raises difficulties in the measurement methodology. In the case of [40], K_H = 2.67 W.s and K_E = 0.00107 W.s^2. The maximum motor efficiency η_{motor_max} is read from the tables, depending on the rated motor power. The most plausible table is the one with maximum motor efficiency of around 90% for a 32 kW motor. For a 4.5 kW motor used in the DELTA 4.5 OMLAT Electrobrush (fig. 3.6) this value is around 80%.

$$\eta_{motor} = \eta_{motor\_\max} \cdot \eta_{spec\_speed} \cdot \eta_{spec\_load}, \tag{3.26}$$

$$\omega_{motor\_rel} = \frac{\omega_{motor}}{\omega_{motor\_\max}}, \tag{3.27}$$

$$load_{motor\_rel} = \frac{T_{motor}}{T_{motor\_\max}}. \tag{3.28}$$

In the manufacturer's technical specifications, a maximum rated torque of 3.6 Nm, a friction torque between 0.09 Nm and 0.36 Nm will produce a range between 2.5% and 10% for no-load idling.

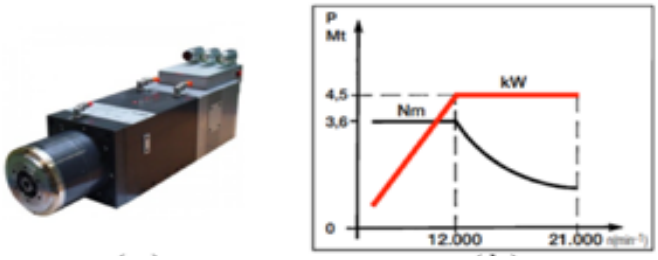

a b

Fig. 3.6. DELTA 4, 5 OMLAT electric broach: *a* - view of the assembly; *b* - torque, power diagram, depending on speed (DELTA 4,5 OMLAT catalog)

The adimensional power coefficient of speed η_{spec_speed} is established from experimental data from the manufacturer with a linear type relationship: $\eta_{spec\_speed} = a + b \cdot \omega_{motor\_rel}$,

$$\eta_{spec\_speed} = 0.83 + 0.08 \cdot \omega_{motor\_rel}. \tag{3.29}$$

The adimensional efficiency coefficient of the load η_{spec_load} can be interpolated from a table which is extracted according to [18] from [106] and which according to the author is in accordance with experimental data presented by [15], but also with data from table 3.2.

Table 3.2 The adimensional efficiency coefficient of the load η_{spec_load} (calculated according to [81])

	η_{spec_load}							
	0,01	0,60	0,70	0,83	0,93	0,97	1,0	,96
$load_{motor\_rel}$	0	0,05	0,1	0,2	0,4	0,6	0,8	1,0

Using equations (3.26)–(3.27), calculate the amount of heat generated by the electric motor according to the experimental data collected on the rotor speed and torque.

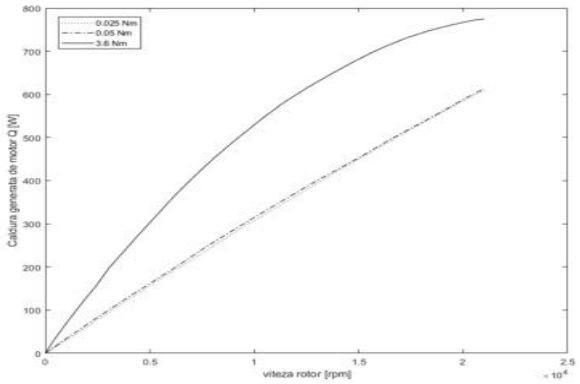

Fig. 3.7 Heat generated by the electric motor of the DELTA 4,5 OMLAT electric broach (own results obtained by calculation with MATLAB)

While the speed is relatively easy to measure, the torque must be determined from the friction in the bearings, the losses from the rotor-air friction, the cutting process and the acceleration.

$$\dot{Q}_{motor} = \omega_{motor} \cdot T_{motor} \cdot \eta_{loss\_motor} = 2 \cdot \pi \cdot f_{motor} \cdot T_{motor} \cdot \frac{1-\eta_{motor}}{\eta_{motor}}. \tag{3.30}$$

For a 4.5 kW motor, DELTA 4,5 OMLAT with a speed between 0–21 000 rpm and a graphical representation for a torque of 0.025 Nm, 0.05 Nm and very close to a maximum torque of 3.6 Nm, the results of fig. 3.7. According to equation 3.25, the nominal frequency for the motor considered in the study, DELTA 4, 5 OMLAT, is different from the value 833 in the example [81]:

$$f_{\text{nominal}} = (N_{\max} \times f)/n_{\text{sync}} = (21000 \times 50)/1500 \approx 700 \text{ Hz}. \tag{3.31}$$

Slippage is defined as the ratio of the change in speed to the change in torque. The heat fraction of all electric motor losses is modeled by:

$$\dot{Q}_{rotor} = \dot{Q}_{motor} \cdot \frac{f_{slip}}{f_{sync}}, \tag{3.32}$$

$$\dot{Q}_{stator} = \dot{Q}_{motor} - \dot{Q}_{rotor}, \tag{3.33}$$

$$f_{slip} = \frac{(n_{sync} - n_{rotor}) \cdot P}{120}. \tag{3.34}$$

The air in the small space between the moving rotor and the fixed stator is heated, and this heat is transported by the air flow to the outside. We can approximate in small portions that the two surfaces are flat.

For a Newtonian fluid such as air, the friction force is given by the relation:

$$\tau = \mu_{aer} \cdot \frac{\partial u}{\partial y} = \mu_{aer} \cdot \frac{\omega_{rotor} \cdot \frac{d_{rotor}}{2}}{h_{gap}} \tag{3.35}$$

where $\mu_{air} = 18.5 \cdot 10^{-6}$ [Ns/m^2] is the dynamic viscosity of the air, u - represents the velocity of the air in the direction of the circumference (boundary), *y* - the radial coordinate (height above the boundary), ω_{rotor} – rotation frequency ($\omega = u / r$, *r* – radius that is approximated by linear values), d_{rotor} –rotor's diameter and h_{gap} – the gap between the rotor and the stator. Rotational torque at a given speed and rotor frequency f_{rotor} (we consider the rotor a cylinder of length l_{rotor}) is:

$$T = r_{rotor} \int \tau dA_{rotor} = \frac{\pi \cdot d_{rotor}^3 \cdot l_{rotor} \cdot \mu_{aer} \cdot f_{rotor}}{2 \cdot h_{gap}}, \tag{3.36}$$

where A_{rotor} represents the surface of the cylinder which is the rotor. The power lost by viscous friction with air is given by:

$$P = \omega_{rotor} \cdot T = \frac{\pi^3 \cdot d_{rotor}^3 \cdot l_{rotor} \cdot \mu_{aer} \cdot f_{rotor}^2}{h_{gap}} \tag{3.37}$$

The data of the 4.5 kW DELTA 4.5 OMLAT motor are: d_{rotor} = 74,3 mm; l_{rotor} = 120 mm; h_{gap} = 0,3 mm; n_{rotor} = 0–21000 rpm; Frequency $f_{rotor} = n_{rotor}$ / 60 Hz, namely f_{rotor} = 0–350 Hz. The kinematic viscosity of the air varies with temperature. For example, for 18ºC, ν_{air} = 14,88·10^{-6} [m^2/s] and for 70 °C, ν_{air} = 19,86·10^{-6} [m^2/s], as a result for the interval 18– 70ºC in which we consider the normal working temperature, we can consider the constant ν_{air} = 14,88·10^{-6} [m^2/s]. With the data of the 4.5 kW DELTA 4, 5 OMLAT motor and an air flow between 0 [m3 / s] and 4*10-3 [m3 / s], results the theoretical curves in Figs. 3.10, simulation performed with Matlab / Simulink.

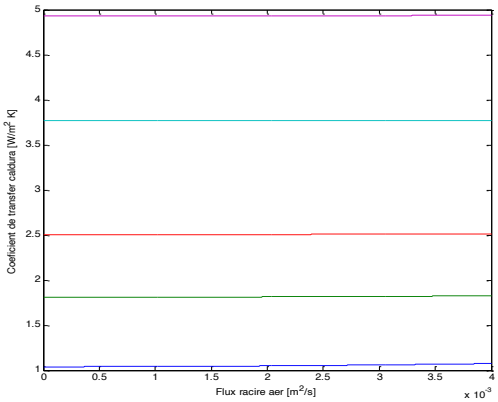

Fig. 3.10 Heat transfer coefficient for air cooling of the motor at ambient air pressure

We will use the methodology [81] for our particular case, helical cooling circuit for main shafts with bearings integrated with the electric motor. The coolant (water) flows in a continuous loop through the corresponding helical channel. The helical channel has a rectangular profile. The convection coefficient is dependent on the flow rate at which the cooling water is recirculated, but is independent of the rotational speed of the shaft, because the cooling water is not in direct contact with the surfaces of the shaft and its components. As a result, the velocity profile of the fluid is not affected by the rotational movement of the shaft.

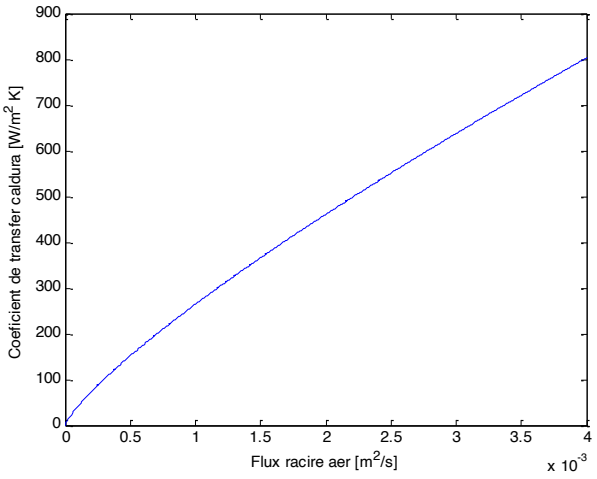

Fig. 3.12. Heat transfer coefficient relative to cooling flow

The heat transfer coefficient in steady state between the housing's surface and the air is assumed to be 9.7 [W / m^{2}K], a value taken from the literature. For ambient air that rotates at the output of the shaft to the tool holder, the heat transfer coefficient can be approximated with a quadratic function [81], Fig. 3.12:

$$\alpha = (9.7 + 5.33 \cdot v_{\text{sup}rafata}^{0.8}), \tag{3.46}$$

where $v_{surface}$ –the average speed at the shaft exit is dependent on the shaft rotation. Air convection in a bearing (here we refer to angular contact bearings), is determined by the air contact surface comprising the Z-ball surfaces, the inner ring surface and the outer ring surface:

$$A_{\text{suprafata}} = A_{inel\_interior} + A_{inel\_exterior} + Z \cdot A_{bila} = \frac{\pi}{4} \cdot d_i^2 + \frac{\pi}{4} \cdot d_o^2 + Z \cdot \pi \cdot D_b^2 . \tag{3.47}$$

The heat transfer coefficient is approximated with the relation [27], fig. 3.5:

$$\alpha = (9.7 + 5.33 \cdot \bar{u}^{.8}) \frac{W}{m^2 K} \tag{3.50}$$

In encapsulated bearings, these assertions are no longer valid, the balls being insulated from the outside by caps (usually the insulation is made of plastic or rubber). In this case we will consider that there is no convection with air in the bearings.

3.3. THERMAL DEFORMATIONS AT THE LEVEL OF THE MAIN SHAFT-BEARINGS

The shaft-bearing structure in dynamic regime, is deformed due to the centrifugal forces and due to the increase of the temperature generated mainly by the friction phenomenon in bearings to which is possibly added the heat generated by the electric motor, in the case of motorized assemblies. Radial and axial displacements are inherent with increasing temperature and in practice are very difficult to measure.

When a solid body is subjected to a higher temperature, the body volume increases due to the phenomenon of expansion. In solids, molecules are located next to each other, contributing to the shape of that solid (and surfaces). When the temperature of the solid increases, the molecules tend to vibrate faster and move away from each other, the kinetic energy of the material increases, so the volume of the structure increases.

Since the temperature varies along the shaft (the heat sources are the bearings), an approximate formula is chosen, the value of the temperature on a segment being the average value of the temperature at the ends of the shaft. Since the variations of the angle depending on the rotation speed are nonlinear, and the variation of the shaft length will have a nonlinearity, even if the slope is smaller, due to the contribution given by the two segments xfr = 65.7 mm and xfl = 75.4 mm (Fig. 3.18).

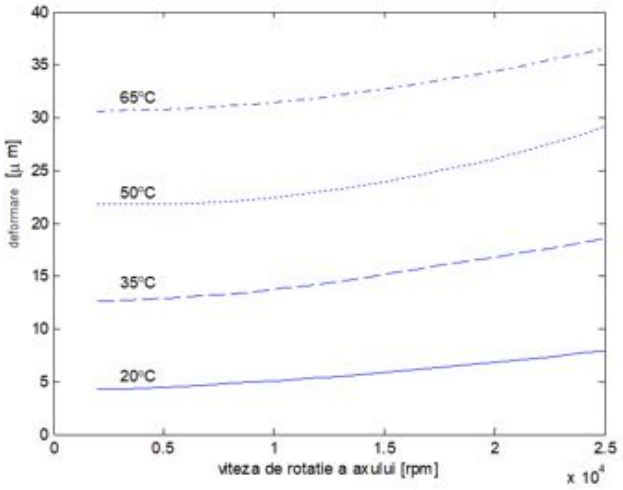

Fig. 3.18. Axial deformation as a function of rotational speed

3.4. MODELS OF THE BEARING SHAFT USING THERMAL NETWORKS

In the practical case with axial radial ball bearings with angular contact, the formulas (3.51) - (3.54) are used, having as variables the material used (steel balls or ceramic material fig. 3.19–3.20), geometry, number of balls, lubricant, force pretensioning / preloading (dynamic ball-bearing contact angle) and the model used, if for example the gyroscopic effect is considered (Fig. 3.21a–3.21b).

.

$$R_{1ri} = R_{0ri}[1+\alpha_T \cdot (T_r - T_0)];$$
$$R_{1ro} = R_{0ro}[1+\alpha_T \cdot (T_r - T_0)]; R_{1s} = R_{0s}[1+\alpha_T \cdot (T_s - T_0)]. \quad (3.51)$$

$$R_{2ri} = R_{1ri} \cdot \left(1 + \frac{[(3+\nu)R_{1ri}^2 + (1-\nu)R_{1ri}^2]\rho_r \omega_s^2}{4E}\right), \quad (3.52)$$

$$R_{2ro} = R_{1ro} \cdot \left(1 + \frac{[(1-\nu)R_{1ro}^2 + (3+\nu)R_{1ro}^2]\rho_r \omega_s^2}{4E}\right), \quad (3.53)$$

$$R_{2so} = R_{1so} \cdot \left(1 + \frac{(1+2\nu)R_{1so}^2 \rho_r \omega_s^2}{4E}\right) \quad (3.54)$$

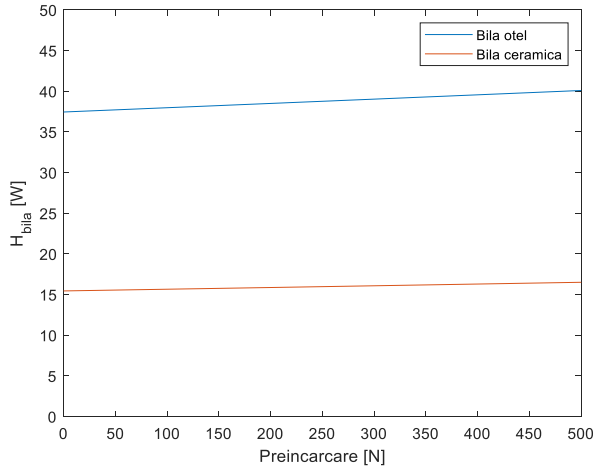

Fig. 3.19. Heat generated by a steel ball compared to ceramic ball with the same diameter, in

bearings with the same geometric dimensions, preload function, preload interval 0–500 N, bearing dimensions

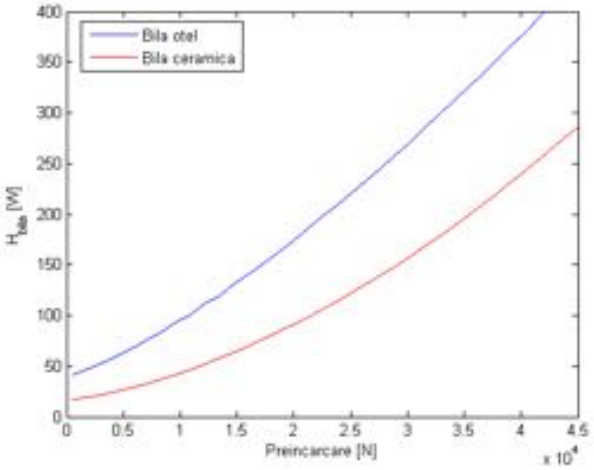

Fig. 3.20. Heat generated by a steel ball compared to ceramic ball with the same diameter, in bearings with the same geometric dimensions, preload function, extended preload interval (according to the practice in the literature) 0–45 000 N, bearing dimensions

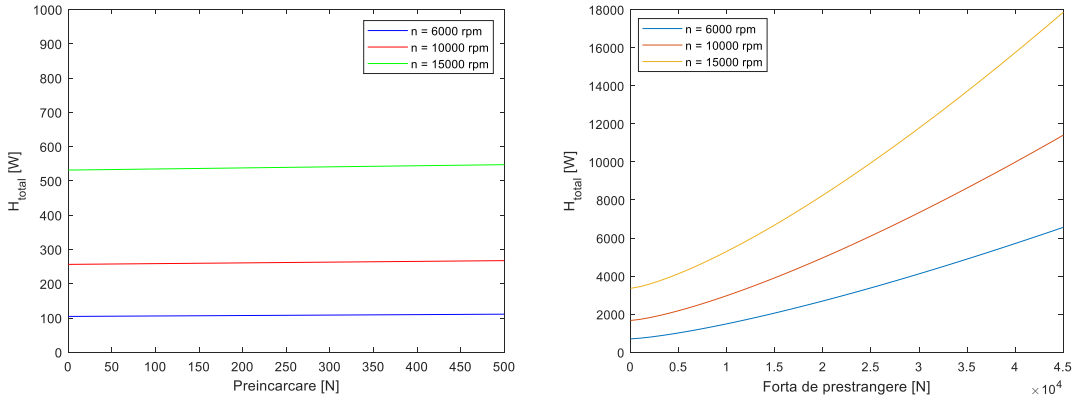

a b

Fig. 3.21. Heat generated: a - by a bearing with angular contact with Z = 25 balls, preload function, preload interval 0–500 N (a); b - of an angular contact bearing with Z = 25 balls, preload function, extended preload range (according to the practice in the literature) 0–45 000 N, bearing dimensions

Tabelul 3.3. Heat generated by a bearing with angular contact with Z = 25 balls, bearing dimensions ≈in [W]

	F_p [N]									
n [rpm]	0.0	100.0	500.0	1000.0	3000.0	6000.0	10000.0	20000.0	30000.0	45000.0
6000	715,6	720,5	740,9	768,4	897,4	1136,7	1518,4	2691,7	4103,7	6565,6
10000	1664,0	1673,2	1711,1	1760,7	1982,9	2379,0	3004,6	4937,2	7271,8	11358,2
15000	3402,0	3413,4	3461,3	3526,1	3834,2	4412,8	5341,0	8202,6	11680,8	17890,5

A tabular representation of the data in fig. 3.21, for n = 6000 rpm, with rounding to the first two decimal places is given in table 3.3. We consider for a preliminary analysis the angular contact bearings and the geometric data used for the case in Fig. 3.22, a section element with a single bearing, located in the right position, extreme.

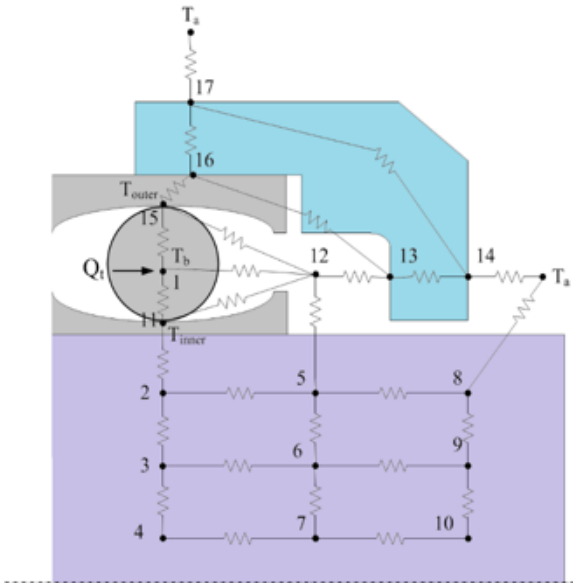

Fig. 3.22 Partial thermal network for a model of bearing, shaft, housing, with the representation of geometric components

We use a model adapted to the situation in fig. 3.22. The bearings have the geometric dimensions: (a) 7014 CETNH / HCP4AQBCA angular contact balls, d = 70 mm, D = 110 mm, B = 20 mm, Z = 25, and axial stiffness kax = 120 N / µm; (b) N1012 RGT42KRCC1P4, with cylindrical rollers, d = 60 mm, D = 95 mm, B = 18 mm, Z = 20, roll length L = 9 mm.

The amount of heat generated by the bearing (table 3.3) will be divided into two equal amounts or will be punctual, in the concrete case studied (the two common approaches in the literature). By similarity to Kirchoff's laws we will write the equilibrium equations for each node (17 equations, the temperatures in the nodes representing the unknown quantities, (fig. 3.22).

The unknowns are T_i, i = 1, ..., 17 and T_a = 25,5 °C – ambient temperature, outside air temperature. Note that the resistors $R_{17,19}$, $R_{14,19}$ şi $R_{8,18}$ are convective resistors, as a result of the corresponding convective conductances $K_{17,19}$, $K_{14,19}$ şi $K_{8,18}$ belong to vector b, together with the heat source Q. Finally, the system of equations must look like this $K \cdot T = b$ with the solution $T = K^{-1} \cdot b$ where K represents the matrix of conductors and b the sources of heat or cooling (including ambient temperature).

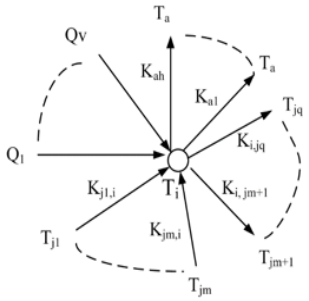

Fig. 3.24 A termal node: $Q_1 ... Q_v$ – heat sources; $T_{j1} ... T_{jm}$ inputs from previous nodes; $T_{jm+1} ... T_{jq}$ outputs to other nodes; T_a – output nodes to ambient temperature (all nodes have the same T_a but have different K conductances, $K_{a1}, ..., K_{ah}$)

In order to automatically implement the thermal network, it is necessary to find a form of calculation of the matrix K and b without going through the equations of the nodes, namely, directly the line of the matrix K in the equation of this node. We denote the nodes of the network from 1 to N_t, N_t being the total number of nodes. The equation of the general node in fig. 3.24 can be written using Kirchoff's theorem 1 as:

$$K_{j1,i}(T_{j1}-T_i)+\ldots+K_{jm,i}(T_{jm}-T_i)-K_{i,jm+1}(T_i-T_{jm+1})-\ldots$$
$$-K_{i,jq}(T_i-T_{jq})-K_{a1}(T_i-T_a)-\ldots-K_{ah1}(T_i-T_a)=Q_1+\ldots+Q_v, \quad (3.96)$$

$$K_{j1,i}\cdot T_{j1}+\ldots+K_{jm,i}T_{jm}+K_{i,jm+1}T_{jm+1}+\ldots+K_{i,jq}T_{jq}$$
$$-(K_{j1,i}+\ldots+K_{jm,i}+K_{i,jm+1}+\ldots.+K_{i,jq}+\ldots K_{a1}+\ldots.+K_{ah1}), \quad (3.97)$$
$$\cdot T_i=Q_1+\ldots+Q_v-(K_{a1}+\ldots.+K_{ah1})\cdot T_a$$

$$k_{j1,i}\cdot T_{j1}+\ldots+k_{jm,i}T_{jm}+k_{i,jm+1}T_{jm+1}+\ldots+k_{i,jq}T_{jq}-$$
$$k_{ii}\cdot T_i=Q_1+\ldots+Q_v-(K_{a1}+\ldots.+K_{ah1})\cdot T_a \quad . \quad (3.98)$$

where:

$$\begin{bmatrix} k_{11}\ k_{12}\ldots k_{1n} \\ k_{11}\ k_{12}\ldots k_{1n} \\ \vdots\ \ \vdots\ \ \ \vdots \\ k_{n1}\ k_{n2}\ldots k_{nn} \end{bmatrix}\begin{Bmatrix} T_1 \\ T_2 \\ \vdots \\ T_n \end{Bmatrix}=\begin{Bmatrix} b_1 \\ b_2 \\ \vdots \\ b_n \end{Bmatrix}. \quad (3.99)$$

From equations (3.96)–(3.99), it is easy to identify the indices in the matrix K and the corresponding values of the conductances, identifying the nodes adjacent to the node of interest T_i where i is the index of the node in the total number of nodes. We propose an original matrix construction algorithm $K=[k_{ij}]_{i=1,\,n\,;\,j=1,\,n}$ based on simple observations so far.

The system of equations is given by the Kirchoff equilibrium equations for each node and, if we have built the network, with the numbered nodes, the oriented graph edges and the K_{ij} conductances between the calculated nodes. Having the matrix *K* and the matrix *b*, solving the system of linear equations $K*T=b$, can be done either with iterative methods (Gauss-Seidel) or simply, using Matlab, $T=K\setminus b$.

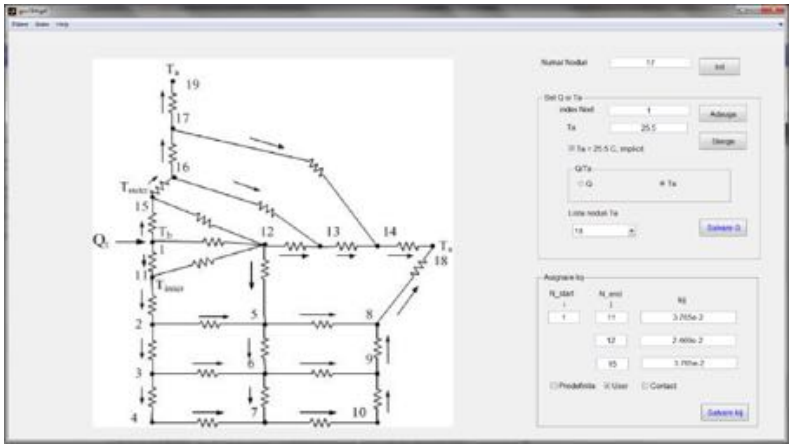

Fig. 3.25 GUI, introduction of ambient temperature points and conductors for the calculation of the matrix *K* and the vector *b*

Step 1 Array initialization K, of size n x n with the value zero, where n is the total number of nodes.

Step 2 For each line *i*, calculate the line of conductors k*ij* using the equations (3.96)–(3.99)

Step 3 For each line *i*, calculate term b_i according to the ecuation (3.96)

In the preliminary research, we propose a graphical user interface (GUI) for the construction of the graph that represents the thermal network (fig. 3.25). The simulation results for a heat source of 276.43 W, corresponding to a pre-clamping force of 300 N at an axis speed

of 2,000 rpm. The accuracy of the model will clearly depend on the level of discretization for the thermal network in the case of the bearing shaft. By comparison, a level of 1,000 tetrahedral elements for finite element modeling will produce an accuracy very close to reality, but thermal network modeling with 1,000 knots is very difficult to perform manually..

3.5 OPTIMIZING THE DURABILITY OF ANGULAR CONTACT BALL BEARINGS ACCORDING TO THE WORKING PARAMETERS OF THE MAIN SHAFT

We take into account the fact that the bearing shaft and the housing have the geometry and characteristics of the materials preset by the manufacturer. The location of the bearings is also given by the manufacturer. As such, there are few elements that can be investigated to optimize the operation of the shaft. One of the important parameters in optimization is the durability of the main shaft-bearings assembly which is mainly dependent on the durability of the bearings. Radial-axial ball bearings with angular contact are the ones that essentially determine this durability. In order to make a calculation estimate on durability we will propose and develop the methodology from chapter 18 of [23] with the algorithm proposed in Fig. 3.27.

$$L = \left(L_i^{-e} + L_o^{-e}\right)^{-1/e} \tag{3.100}$$

where $e = 10/9$ for angular contact bearings and $e = 9/8$ for roller bearings (linear contact cylinder, L_i – durability of the ring that rotates and L_o – static ring durability.

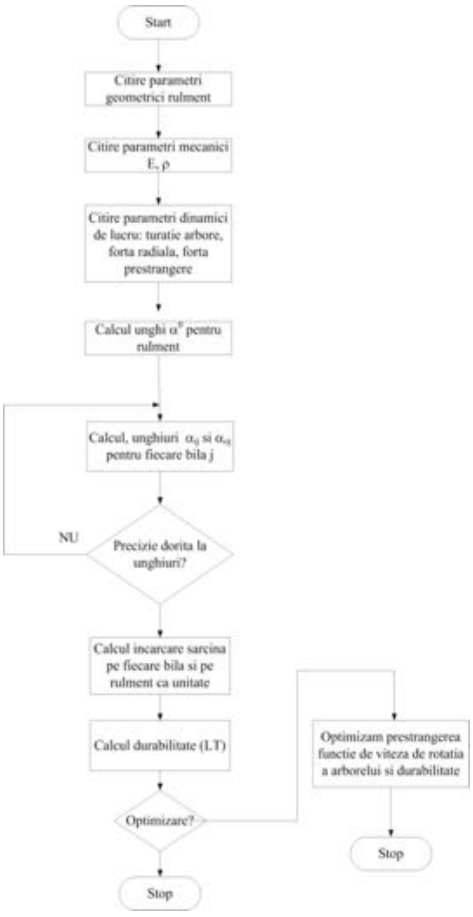

Fig. 3.27. Logic scheme of the algorithm

For angular contact bearings, keeping the notation Q for the force applied to the ball (it will be the sum of the forces for Z balls), the formula becomes:

$$L = \left(L_i^{-10/9} + L_o^{-10/9}\right)^{-9/10}, \tag{3.101}$$

$$L_i = \left(\frac{Q_{ci}}{Q_{ei}}\right)^3, \tag{3.102}$$

$$Q_c = 9.81\left(\frac{2f}{2f-1}\right)^{0.41} \frac{(1\mp\gamma)^{1.39}}{(1\pm\gamma)^{1/3}}\left(\frac{\gamma}{\cos\alpha}\right) D^{1.8} Z^{-1/3}, \tag{3.103}$$

$$Q_{ei} = \left(\frac{1}{Z}\sum_{j=1}^{j=Z} Q_j^3\right)^{1/3} \tag{3.104}$$

Durability L is calculated in millions of rotations and noting with n the speed of the shaft in rpm, L in hours is given by: $LT = \frac{L}{60 \cdot n}$. The balls are made of steel, but in the case of ceramic balls, both the mass of the balls, the constant of the material, and the centrifugal force and moments will change.

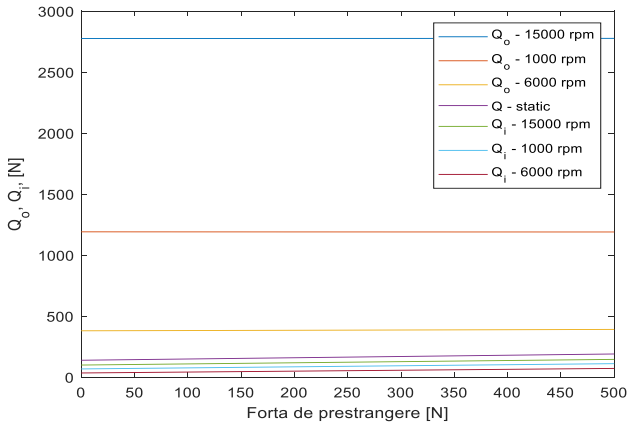

Fig. 3.28. Nominal load on an angular contact ball bearing, Qi and Qo as a function of speed and pre-tightening force (step 4 of the algorithm), pre-tightening range [0 500] N

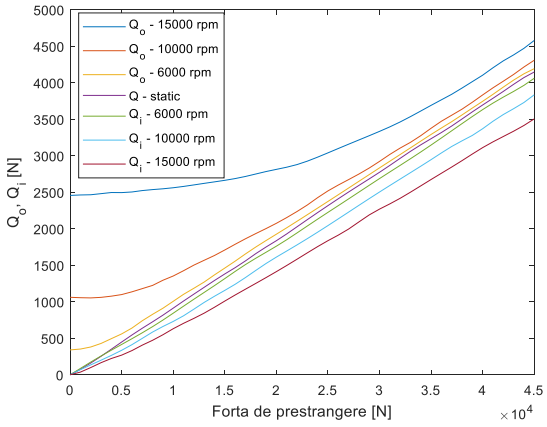

Fig. 3.29. Nominal load on an angular contact ball bearing, Qi and Qo as a function of speed and clamping force (step 4 of the algorithm), extended clamping range [0 4.5 × 104] N

The balls are made of steel, but in the case of ceramic balls, both the mass of the balls, the constant of the material, and the centrifugal force and moments will change. As a result, the inner and outer angles of the ball contact with the inner and outer rings are expected to be smaller. The calculated LT service life is given in Fig. 3.30–3.31.

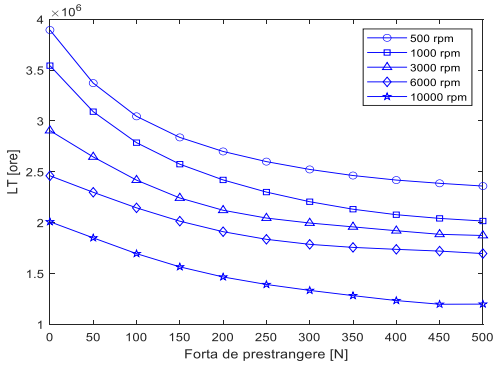

Fig. 3.30. LT depending on the clamping force and the rotational speed of the shaft in dynamic mode, the clamping range [0 500] N

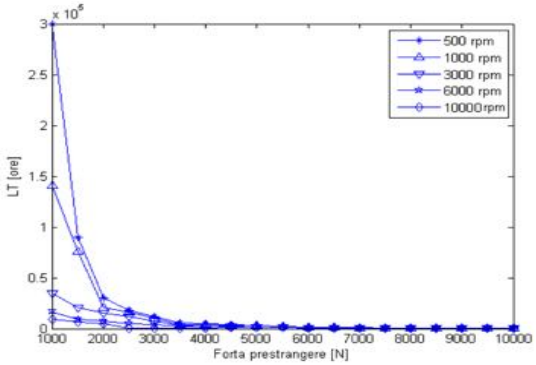

Fig. 3.31. *LT depending on the clamping force and the rotational speed of the shaft, in dynamic mode, extended prestressing range [0 4,5 × 104]*

Pre-tightening is useful in practical cases up to 400–500 N, maximum values also recommended by manufacturers. Following the results of Fig. 3.19, Fig. 3.21, Fig. 3.28 and Fig. 3.30 were presented for pre-constraints in the field [0 500] N. In papers that publish research in the field of the thesis, the results apply to a wide field, 0–4.5 × 104 N, even if not currently applied in practice and according to them Fig. 3.20, Fig. 3.21, Fig. 3.29 and Fig. 3.31.. The optimization variant usually used is a function of durability. Select a rotational speed from which the pre-tightening force is deduced. However, if we consider that durability and rotation speed are variables that come into play, then we can determine the clamping force in the graph in fig. 3.30–3.31 and tabular in table 3.4.

Table 3.4 *LT* depending on the pre-tightening (Fp) and the rotational speed of the shaft, graphic (fig. 3.30)

	F_p [N] × 10^6										
N [rpm]	0	50	100	150	200	250	300	350	400	450	500
500	3,89	3,37	3,04	2,84	2,70	2,60	2,52	2,46	2,41	2,39	2,36
1000	3,54	3,09	2,78	2,57	2,41	2,30	2,21	2,13	2,08	2,04	2,02
3000	2,90	2,65	2,42	2,24	2,12	2,04	1,99	1,96	1,92	1,88	1,87
6000	2,46	2,30	2,14	2,01	1,91	1,83	1,79	1,76	1,74	1,72	1,69
10000	2,01	1,85	1,69	1,56	1,47	1,39	1,33	1,28	1,23	1,19	1,19

Linear or nonlinear optimization algorithms, with or without constraints, based on gradient or free-derivatives are very suitable for a problem with a small number of variables (2–8). However, the biggest difficulty is the definition of the objective function. A proposed formula can be a weighted linear combination (of weights w_1 and w_2, subunit with $w_1 + w_2 = 1$) of the two objectives, a solution of multi-objective type:

$$f_{cost} = w_1 \cdot f_1 + w_2 f_2, \quad f_1 = 1/LT, \quad f_2 = 1/speed, \tag{3.106}$$

3.6 OPTIMIZATION OF MAIN SHAFTS WITH BEARINGS BASED ON A SELECTION OF WORKING PARAMETERS AND A THERMOELASTIC MODEL

The original contributions in this section are inspired by [116] and [26]. The optimized approaches are not a combination of the two sources but a new approach to the issue of optimizing the operation of the main shafts with bearings, depending on a selection of parameters of interest involved in the operation.

We will consider a multi-objective approach, with a more complex housing geometry than the one presented in [116] and an optimization of the eigenfrequencies [26] simultaneously with a reduction of the temperature at the level of the shaft and housings. The axial deformations of the shaft produced by the thermo-mechanical phenomena and by the heat generated by the bearing but also by the friction phenomena that modify its geometry therefore lead to changes in the natural frequencies of the shaft-bearings-spacer-bushing-housing assembly.

The speed at which the shaft works is also important, the nominal speed being specified in the literature. For the considered case, in the research we followed the manufacturer's recommendations and we did the study at a nominal speed n = 2,000 rpm (in the literature, the values encountered are 1,200–2,500 rpm). The reasons for the choice are given by the objective of having terms to compare the results obtained with those published in the literature.

Last but not least, the material from which the assembly is made can contribute to a higher durability of the cutting tool containing the main shaft-bearing assembly and to a lower roughness of the machined surface. In our case, the materials are those in the catalog for bearings, shaft and housing. For the rest of the materials (spacers) values were taken from the literature. A series of approximations were made, neglecting the bushes and nuts and the geometric shapes were simplified, resulting in the sizes selected from fig. 3.32–3.33.

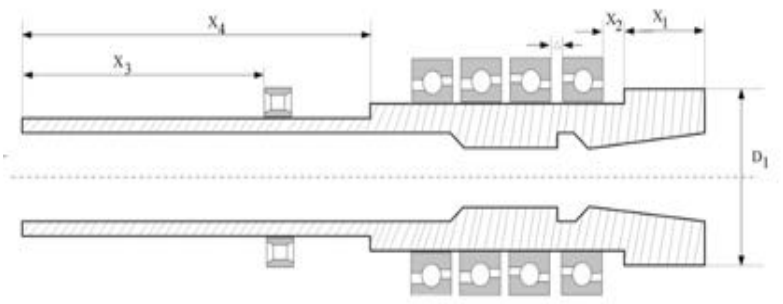

Fig. 3.32 Notations for the geometric dimensions of the main shaft and the positions of the bearings taken into account in the proposed optimization

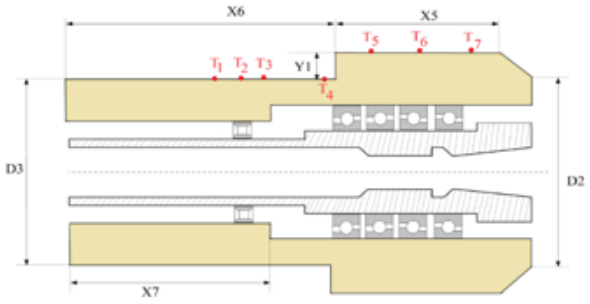

Fig. 3.33 Notations for the geometric dimensions of the housing taken into account in the proposed optimization

In the proposed optimization algorithm, several constraints resulting from construction methods were taken into account, namely the four bearings fig. 3.32-3.33 are mounted in tandem in O, as a result they are considered a single block, determined by a single position variable, namely X_2.

The constraints for all variables taken into account, including the value of the pre-tightening force are:

$$37 \le X1 \le 67 \ \text{(mm)}; \tag{3.108}$$
$$10 \le X2 \le 26 \ \text{(mm)}; \tag{3.109}$$
$$55 \le X3 \le 85 \ \text{(mm)}; \tag{3.110}$$
$$123 \le X4 \le 163 \ \text{(mm)}; \tag{3.111}$$
$$65 \le X5 \le 85 \ \text{(mm)}; \tag{3.112}$$
$$118 \le X6 \le 158 \ \text{(mm)}; \tag{3.113}$$
$$85 \le X7 \le 115 \ \text{(mm)}; \tag{3.114}$$
$$10 \le Y1 \le 20 \ \text{(mm)}; \tag{3.115}$$
$$80 \le D1 \le 100 \ \text{(mm)}; \tag{3.116}$$
$$95 \le D2 \le 125 \ \text{(mm)}; \tag{3.117}$$
$$170 \le D3 \le 210 \ \text{(mm)}; \tag{3.118}$$
$$0 \le F_p \le 850 \ \text{(N)}. \tag{3.119}$$

The vector of variables will look as follows $X = \{X1, X2, X3, X4, X5, X5, X7, Y1, D1, D2, D3, F_p\}$, and the optimization functions are defined by equation (3.107), f_1 and f_2.The complete optimization algorithm with details is described below:

Step 1. Initialization of the individual P population for the variables X, in linear binary coding correspondence for the genetic algorithm, in the constraint domains given by the equations (3.108)–(3.119).

Step 2. Calculate in MATLAB the values of the contact angles for the speed n = 2,000 rpm and the pre-tightening function F_a from the vector X of variables.

Step 3. Calculate in MATLAB the values of the amount of heat generated by the angular contact bearings and the roller bearing.

Step 4. For all individuals in the P population, the following simulations are performed:

Step 4.1. The thermal model of the shaft is simulated in SolidWoks with the predetermined materials and the dimensions given by X. The ambient temperature is considered T_{amb} = 25° C. The temperatures T_i are extracted.

Step 4.2. Calculate the objective function f_2.

Step 4.3. The SolidWoks modal analysis is performed under static conditions, dimensions given by X, without the value F_a (consider the contact angle of the balls without prestressing or axial loading). The values N_1, N_2 and N_3 are extracted.

Step 4.4. Calculate the objective function f_1.

Step 5. Evaluate the functions objectively according to equation (3.107). The individual k in the population with the lowest objective function values is the optimal one and is selected as optimal.

Step 6. If the stop conditions are met, go to Step 12. If the conditions are not met, continue the genetic algorithm with the specific operations.

Step 7. *Individual* selection, *tournament* mode, *elitism* criteria.

Step 8. *Crossover* operations are performed at two points, with probability p_{cross}.

Step 9. *Mutation* operations are performed, with probability p_{mut}.

Step 10. The new population is generated with better performing individuals.

Step 11. Proceed to Step 2.

Step 12. STOP algorithm.

The simulation data were P = 30, p_{cross} =0,35, p_{mut} = 0,01, and the maximum number of generations of up to 25, For each individual in the population, the geometric dimensions of the shaft, housing and bearing location in SolidWorks have been changed for each generation resulting in a new simulation for thermal regime and a new simulation for modal analysis. In total there were 30 □ 25 = 750 different dimensional models that had to be redesigned and simulated in SolidWoks with heat generation calculations in Matlab. The operations were done manually, as a MATLAB Simulink interface is not currently possible for an automated batch run process. The results of the iterations are shown in figs. 3.35–3.38, and table 3.5, resulting in optimal values starting with iteration 20, in other words of the 20th generation of the population.

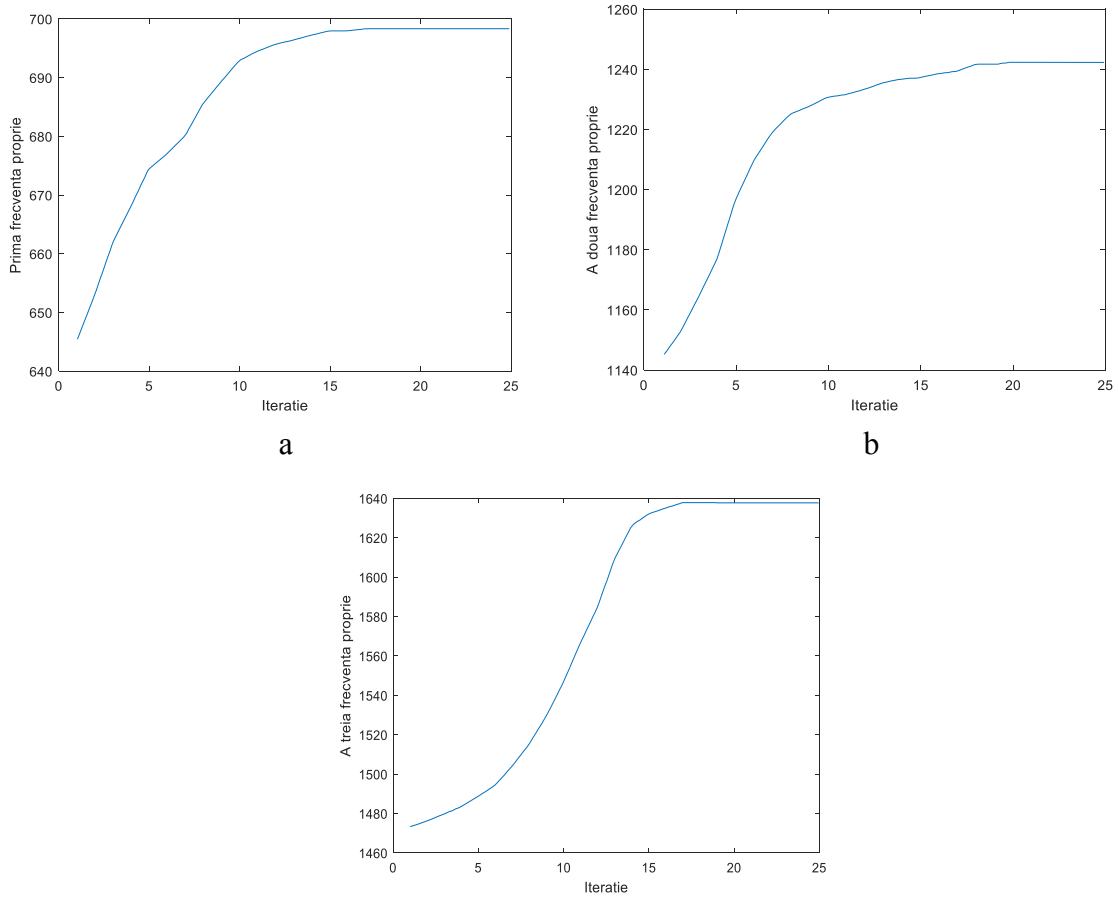

Fig. 3.35. Convergence of eigenfrequencies according to iterations: *a* –first; *b* - the second c-third

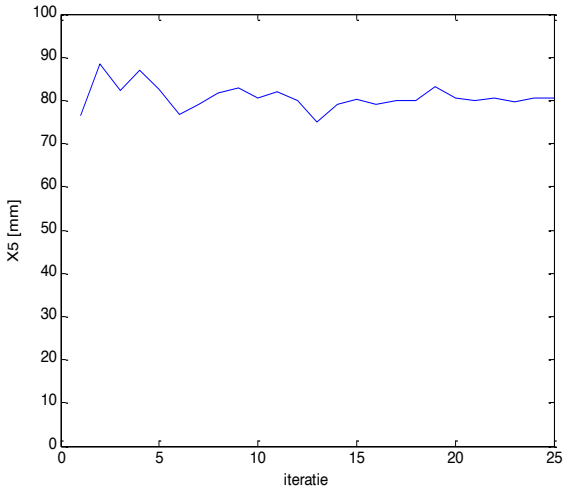

Fig. 3.36. Evolution of parameter X5 depending on iterations

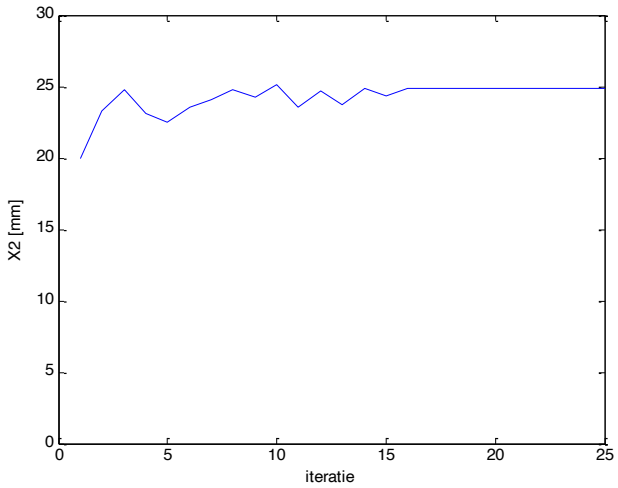

Fig. 3.37. Evolution of parameter *X*2, bearing position depending on iterations

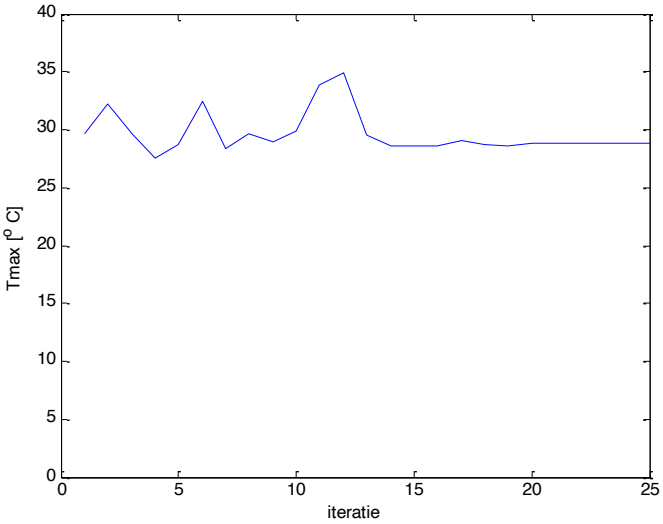

Fig. 3.38. Evolution f_2 (mixed temperatures) în depending on iteration

Table 3.5. Table with optimal values of vector X after 25 iterations (geometric dimensions are in mm and F_p is in N)

***X*1**	***X*2**	***X*3**	***X*4**	***X*5**	***X*6**	***X*7**	***Y*1**	***D*1**	***D*2**	***D*3**	F_p
53,21	24,91	68,34	146,1	80,53	121,6	101,67	16,25	90,62	169,44	196,2	683

The convergence of algorithms is ensured by the theory behind them and, as a result, the option is not critical for the selection of the algorithm; the critical time is given by the construction of the models. On the other hand, the function f_2 can have several forms, depending on how we define the optimal temperature at which the main shaft works, given several observation points T_i, located in areas where the temperature is highest. These aspects and other forms of the f_2 function will be developed in future research.

3.7. CONCLUSIONS

The shape of the segments from which the shaft is constructed, if there is a wide variety of sizes and conical or frustoconical elements, involves many stiffness matrices that assembled will generate a system of equations with very large matrices with laborious iterative calculations, and solutions whose convergence it can involve many steps.

To optimize the parameters according to variables, we will develop a solution based on genetic algorithms that will be used using other variables, such as temperature.

As a result of these preliminary results, new problems to study and optimization requirements arise, such as bearing or shaft durability requiring complex methods of solving in accordance with the experimental results to be recorded with sufficient accuracy for a valid functional model.

CHAPTER 4
CONTRIBUTIONS ON OPTIMIZING THE FUNCTIONAL BEHAVIOR OF MAIN SHAFT ASSEMBLIES FOR HIGH SPEEDS

4.1. CONTACT ANGLE CALCULATION ALGORITHMS FOR ANGULAR CONTACT BALL BEARINGS USING GENETIC TECHNIQUES

As presented in previous chapters, the system of interdependent and nonlinearly dependent equations with respect to other algebraic equations considers as unknown variables the vector X = {X_{1k}, X_{2k}, δ_{ik}, δ_{ok}} where δ is the notation for the elastic deformation of the ball bearing. The currently used method is the Newton-Raphson numerical method or some forms that are based on derivative techniques and the Jacobian can be used to update the values of the vector X on each iteration until the desired error of the solutions is reached.

The model from fig. 4.1 for the resolution of which it is proposed to use a genetic algorithm with immigration operator (GAMI).

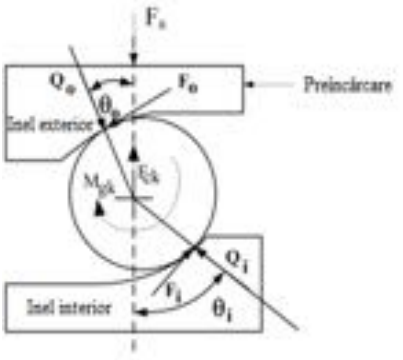

Fig. 4.1. Model of a ball bearing with angular contact, the relationship between the center of the ball and the radii of curvature inner / outer ring

$$(A_{1k} - X_{1k})^2 + (A_{2k} - X_{2k})^2 - \Delta_{ik}^2 = f_1 = 0, \tag{4.1}$$

$$X_{1k}^2 + X_{2k}^2 - \Delta_{ok}^2 = f_2 = 0, \tag{4.2}$$

$$Q_{ok}\cos\alpha_{ok} - \frac{M_{gk}}{D}\sin\alpha_{ok} - Q_{ik}\cos\alpha_{ik} + \frac{M_{gk}}{D}\sin\alpha_{ik} - F_{ck} = f_3 = 0, \tag{4.4}$$

$$Q_{ok}\sin\alpha_{ok} + \frac{M_{gk}}{D}\cos\alpha_{ok} - Q_{ik}\sin\alpha_{ik} - \frac{M_{gk}}{D}\cos\alpha_{ik} = f_4 = 0, \tag{4.4}$$

where Q is the load on each ball (the force acting on each ball depending on the position of the ball), we note with $[a_{ij}]$ the Jacobian of equations (4.1) - (4.4). The update to step n + 1 depending on step n is:

$$\{X^{n+1}\} = \{X^n\} - [a_{ij}]^{-1}\{Y^n\},\ \{y\} = \{y_1\ y_2\ y_3\ y_4\}^{-1} \tag{4.5}$$

Convergence is strongly dependent on the initial values. In this case they are not easy to choose and do not take into account constraints (the trigonometric values sin and cos must be in the range [−1, 1]). Genetic algorithms are meta-heuristic processes inspired by the process of natural selection based on Darwin's evolutionary theory. A GA-type algorithm requires a representation of the solution of the problem, through a chromosome (sometimes called a genotype) which is a set of parameters that define a proposed solution to the problem that the genetic algorithm is trying to solve. The set of all solutions is known as population. The fitness (performance) function is the one that evaluates the range of solutions and calculates the optimal value for each chromosome.

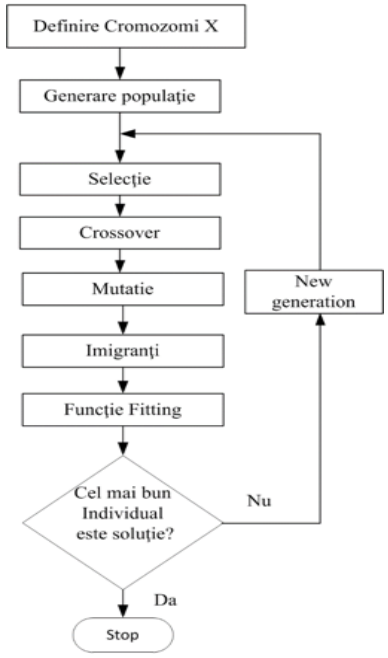

Fig. 4.2. GA block diagram for solving system of nonlinear equations with multiple dependencies (GAMI)

The set of equations (4.1) - (4.4) is transformed into an objective function (the minimum of the objective function, which must be zero, where the terms $f_1 = 0$, $f_2 = 0$, $f_3 = 0$ and $f_4 = 0$ are the terms to the right of the equations (4.1) - (4.4), dependent on the vector $X = \{X_{1k}, X_{2k}, \delta_{ik}, \delta_{ok}\}$) using the absolute value *abs*:

$$f_{fitness} = \text{abs}(f_1(X) + f_2(X) + f_3(X) + f_4(X)), \tag{4.6}$$

The GAMI block diagram is described in fig. 4.2. GA operators are the usual ones: Selection, Crossover, Mutation, Immigration (proposed operator). The selection function is based on the Darwinian principle of elitism. The first step is to encode the problem in binary string, with values "0" and "1". Each chromosome will contain four variables $X = \{X_{1k}, X_{2k}, \delta_{ik},$

$\delta_{ok}\}$ and each variable will be encoded on 16 bits (unsigned integer). The variables, which are floating numbers, are binary coded, subjected to GA operators, then the solution is decoded into the float and the fitness function is calculated for each generation.

In order to avoid premature convergence or convergence to a local instead of a global minimum, there are proposals to maintain the diversity of individuals. A common technique for maintaining diversity is, for example, the "niche penalty", i.e. a penalty is required for any group of members who have a certain level of similarity (a niche geometric radius). The operation consists in introducing −X chromosomes, i.e. the negative value of the chromosome removed from the population and replaced with an "immigrant" chromosome, with a different culture (Fig. 4.6). The population remains constant over all generations of GA.

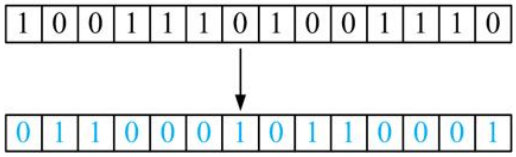

Fig. 4.6. "Immigrant" operator (proposed by the author)

We start with a population of 200 individuals, $p_{crossover}$ = 0,35 $p_{mutation}$ = 0,01, probability of immigration p_{mig} = 0,15 immigration radius r_{img} = 3. After 27 generations (and according to the classical Newton-Raphson algorithm approximately the same error is reached, the fitness function is approximately 0,1 × 10^{-6} (Fig. 4.7).

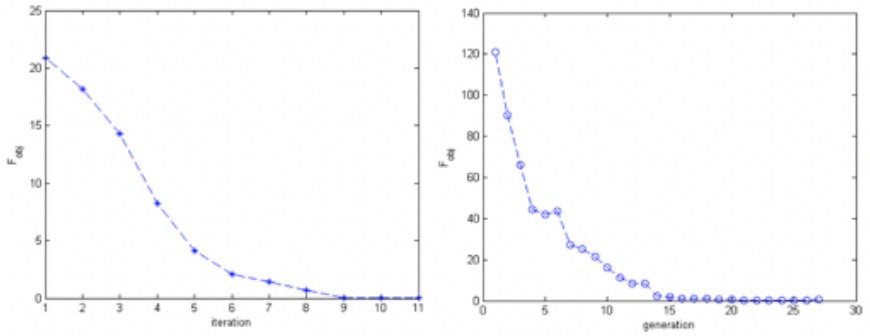

a b

Fig. 4.7. Fitness function: *a* – classical Newton-Raphson algorithm; *b* – GAMI

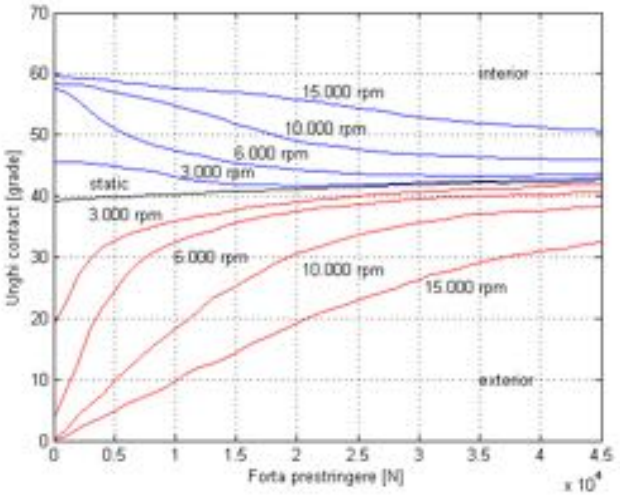

Fig. 4.8. Angles α_i and α_o (for ψ = 0)

Corresponding to these solutions, the values obtained with GAMI are presented in fig. 4.8. It should be noted that this convergence was not obtained from the first application of the algorithms, but from repeated running tests with initial values ("guesses") modified in combinations of 1, 2, 3 and 4 values (corresponding to the variables).

The thermal network method [38], although it requires a greater effort of the user, can be a feasible solution when an analysis of a more complex problem is desired, such as the optimization of the bearings' life.

4.2. SEMI-AUTOMATED MODEL FOR BUILDING A THERMAL NETWORK

In the following, we will use the thermal map of the bearing and the thermal resistances according to the geometry of the regular element (sphere, cylinder, straight circular cylinder, circular cylinder with inner bore), the formulas being given in ([107], [12]).

TCR (Thermal contact resistance) is considered as a function of the shape and size of the contact area between two bodies (in our case two elastic bodies, the ball and the two bearing rings). The contact area is an ellipse, with the semiaxes a and b whose equations are described in ch. 2 and 3 based on the relations in [79]. We consider that the balls and bearing rings are made of the same material (steel), having a coefficient of thermal conductivity of $\lambda = 40–50$ W/(m·K), luăm valoarea medie $\lambda = 45$ W/(m·K).

$$R_{nb} = \frac{\psi(a/b)}{4\lambda a}, \tag{4.8}$$

$$\psi(a/b) = \frac{2}{\pi} K_1\left(e, \frac{\pi}{2}\right), \tag{4.9}$$

where $K_1(e, \pi/2)$ is the elliptic integral of the first case, depending on $k = 1 - (b^2/a^2)$.

$$K_1 = \int_0^{\pi/2} \frac{d\theta}{\sqrt{(1 - k^2 \sin^2\theta)}}, \tag{4.10}$$

RCT for each ball (there are Z balls in the bearing) becomes:

$$R_b = \frac{1}{2\lambda}\left(\frac{\psi(a_0/b_0)}{a_0} + \frac{\psi(a_i/b_i)}{a_i}\right), \tag{4.11}$$

The simulation results are described in figs. 4.9. It is observed that the results are consistent in order of size and values with those of bearings with similar dimensions in the literature. Steel constants were taken from the catalog. The bearing model is that of figs. 4.10.

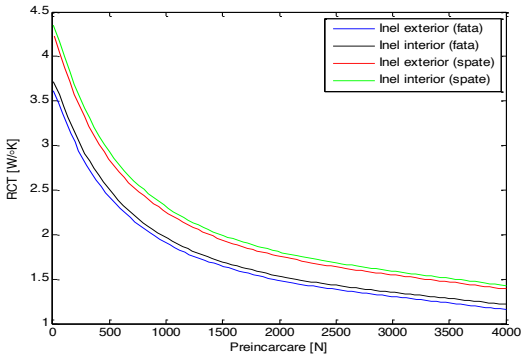

Fig. 4.9. RCT depending on preload, for tandem bearings

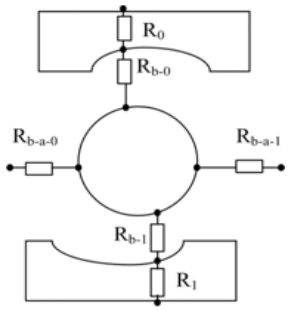

Fig. 4.10. Bearing model with seven contact points: R0, R1 - thermal resistance, *a* - index for air, *b* - index for bearing

In the paper [61], results were published on a proposed method for the semi-automated construction of a thermal network for a shaft with bearings and belt motion transmission. The paper aimed at a software tool for building a supervised thermal network, the construction of a linear generator of symbolic equations that can be solved using numerical software (eg Matlab) in a simpler and less expensive way than software tools using the finite element method.

$$\sum_{k=1}^{4} \frac{T_k - T_i}{R_{ik}} + Q_i = m_i c_i \frac{\partial T_i}{\partial t}, \quad k = \{1,2,3,4\}, \tag{4.12}$$

The center of each block element is marked with a node and the location is described as having the temperature of the entire element. The system of equations is built on the energy balance, the input energy plus the output have the result 0. Ambient temperature has been considered a common value in the literature, $T_a = 25°$ C. Linear thermal resistance and the usual formulas for thermal resistance are: regular body geometries, balls, solid cylinder, hollow cylinder and lubricant resistance (vaseline) [107]:

$$R = L / KA\,, \tag{4.13}$$

$$R_{radial} = \frac{\ln(r_o / r_i)}{2\pi kL}, \quad R_{axial} = \frac{\Delta x}{kA}, \tag{4.14}$$

$$R_b = \frac{1}{k_b \pi r_b}, \tag{4.15}$$

$$R_{Li} = \frac{r_b}{k_l \left(\frac{2\pi}{n} r_i W_i - \pi r_b^2 \right)}, \tag{4.16}$$

$$R_{Lo} = \frac{r_b}{k_l \left(\frac{2\pi}{n} r_e W_e - \pi r_b^2 \right)}, \tag{4.17}$$

Thus, I used a simple partitioning method, inspired by the proposals of other authors, in geometric bodies, mainly cylinders with bore and the taper elements were calculated using the approximate method automatically by partitioning into n cylinders (we currently used n = 10), on a scaled drawing, *.bmp, .tif, or .png* file with simple tool such as Microsoft Paint from

Windows. After partitioning (discretization), the graphical interface (GUI) loads the image and a preprocessing module corrects the vertices of the polygons and the linearity of the right segments.

For example, at three speeds and a variation of the preload between 0 N and 4.5 x 10^4 N, the heat generated by a bearing with angular contact is described in Fig. 4.14.

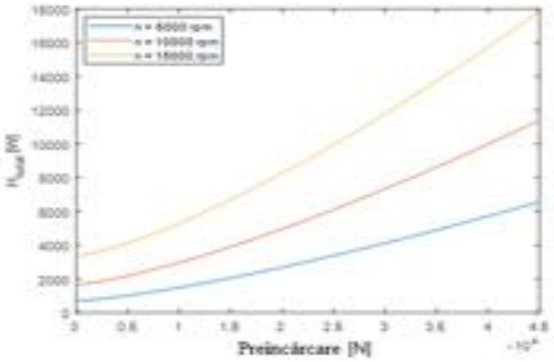

Fig. 4.14. Heat generated by bearing vs. preloading, angular contact bearing

For the heat created by the roller bearing, it is much lower (at 3,000 rpm it is approximately 45 W) and is practically constant in the preload range 0–1 000 N.

For a selection of nodes on the outer surface of the housing, the temperature values corresponding to the selected elements are exemplified in fig. 4.15 temperature values corresponding to the selected elements are exemplified in fig. 4.16.

Fig. 4.15. Manual selection of nodes on the outer surface of the housing for temperature display

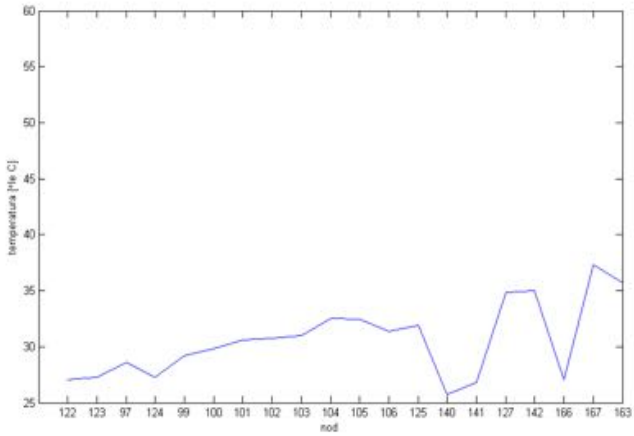

Fig. 4.16. Temperatures on the selecte region 1

4.3. TEMPERATURE – FREQUENCY DEPENDENCE ANALYSIS FOR A BEARING SHAFT

This section describes the personal results obtained by the author and published in the paper [62]. The calculation of natural frequencies plays an important role in the nodal analysis of shaft systems, especially micro-cutting applications specific to the medical field (surgery and dentistry). Each natural frequency is associated with the mass and geometry of the shaft (of course also of the material from which the shaft is built) and the effect of heat transmission generated by friction of bearings causes an axial and a radial expansion of the shaft.

It is known that an increase in the temperature at which the shaft operates affects its performance and reliability over time [183]. These performances are related to reliability, the possibility of defects or a general malfunction. The temperature variation along the shaft length (the shaft is considered symmetrical in section) has the effect of thermal deformation and the calculations are performed for either axial deformation or radial deformation. The general deformation equation is:

$$\Delta L = \alpha L \Delta T\,, \tag{4.18}$$

The results from the literature show for shafts of reasonable length (1–2 m) deformations from a few microns, up to hundreds of microns at low speeds [207]. After a transitional period, in a stable regime, $\Delta T = T_f - T_{amb}$ where T_f represents the final temperature and T_{amb} ambient temperature (in the literature is considered $T_{amb} = 25$ °C or sometimes $T_{amb} = 25{,}5$ °C.

A simple model shaft section with two angular contact bearings and a roller bearing is described in fig. 4.19. In fig. 2.20 the shaft is divided into L_i sections, i = 1, ..., n, where $n = 6$ in this case. The division was made into sections which are regular geometric bodies. A simplified model of bearing shaft, with two angular contact bearings and a roller bearing is in fig. 4.20.

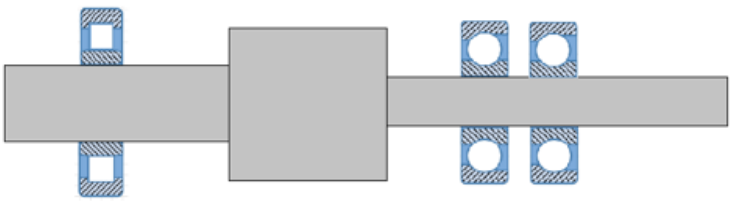

Fig. 4.19. A simplified model of bearing shaft, with two angular contact bearings and a roller bearing

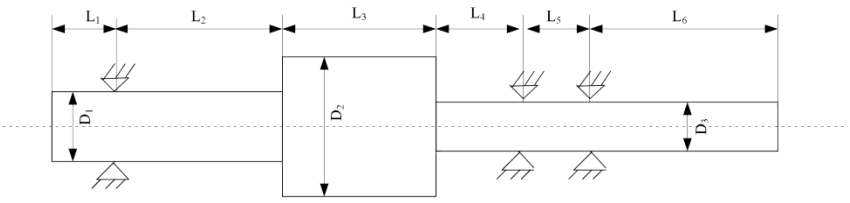

Fig. 4.20. The model used in thermal analysis, the global

stiffness matrix and the modal analysis from the educational instrument proposed by the author in [62].

Due to the complexity of the method, it was not possible to publish it in full in [62], as a result we exemplify the method in the following. Roller bearings (rollers of diameter Dr and length Lr) have contact inner ring / outer ring one line, length Lr. The heat generated by the bearings is given by $Q = u \cdot F_R$, $H = \omega M$ where u represents speed, F_r the friction force, M the torque. In the case of radial cylindrical bearings, we have no pre-tightening force, but only radial force (in our case given the weight of the housing and the shaft) which is distributed on Z rolls.

In the following we use model (2) which although simpler than (3) is more pragmatic for an application such as bearings 7014 CE / HCP4A, small bearings. Consider the fixed outer ring, the movement described by the rotation of the shaft on which the inner ring is fixed, the bearing with cage and flanges on the outside. We note $\gamma = D_w / d_m$, the relative sliding speeds between the rollers and the inner and outer rings which can be expressed in the following form ([24], [33]), for the roller j, if we neglect the sliding phenomenon:

$$v_{ij} = \frac{d_m}{2}\left[(1-\gamma)(\omega_i - \omega_c) - \gamma\omega_{wj}\right], \tag{4.20}$$

$$v_{oj} = \frac{d_m}{2}\left[(1+\gamma)\omega_c - \gamma\omega_{wj}\right]. \tag{4.21}$$

$$M_v = \begin{cases} 10^{-7} f_1 (\nu_0 n)^{2/3} d_m^3 & \text{dacă } \nu_0 n \geq 2000 \\ 160 \times 10^{-7} f_1 d_m^3 & \text{dacă } \nu_0 n < 2000 \end{cases}, \tag{4.22}$$

$$F_c = 3.39 \times 10^{-11} D_w^2 l_t d_m n_m^2, \tag{4.23}$$

$$H_c = F_c v_{io}, \tag{4.24}$$

$$M_g = 8.37 \times 10^{-12} D_w^4 l_t n_R n_m \sin\beta. \tag{4.25}$$

where, f_1 is a factor that depends on the bearing and lubricant (in the case of cylindrical roller bearing, Vaseline, from the table [79] we have the value 0.0002–0.0004, and we choose an average value, f_1 =0,0003), ν_0 represents the kinematic viscosity (depends on the rotation speed of the bearing fixed on the shaft n, and varies in our case and function of lubricant, with a value between 20 and 400 given in the literature, we choose a constant value of 20 centistoke, (valid at low speeds in general).

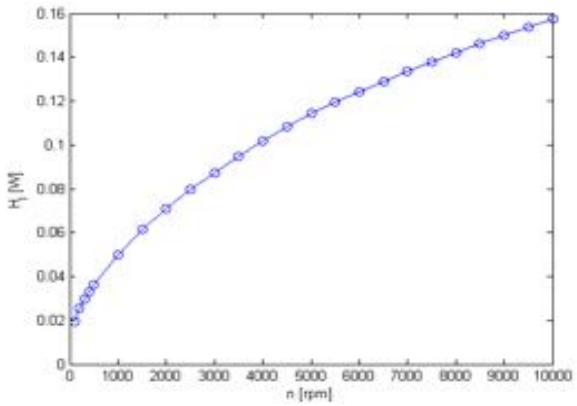

Fig. 4.22. Heat generated by a bearing 7014 CE / HCP4A, for a number of rollers Z = 25

To solve the problem, it is proposed to use a thermal network that calculates the temperature (fig. 4.22) for each element.

The individual frequencies of the shaft-bearing assembly but also of the rotor as an individual component are important, in order to avoid the resonance phenomenon that can lead to important failures, likely to affect the good functioning of the system or to avoid extreme cases that can lead to the destruction of the components. Avoiding this phenomenon can be done as follows: monitoring the rotational speed of the shaft and knowing its eigenfrequencies, when you reach these rotational speeds increase or decrease the speed.

The direct global stiffness matrix GSMA (assembled by the method of all segments) is obtained by the direct stiffness calculation method (DSM), as mentioned, and is the most common implementation in the finite element method (MEF).

The educational software presented in [18], SbfreqAnalizer presents a graphical interface (GUI) that is built in Matlab. The main program allows two options: a simple shaft predefined and construction of a new shaft using tables and dimensions for sections with different shaft diameters. In the first case, the thermal curve is predefined and is calculated for three bearings, for variable shaft rotation speed (predefined or set by the user) between 0 and 6,000 rpm. The material considered is steel with a density p = 7800 kg / m3. This part has a purely educational role and can be used as an introduction together with a related guide which is in pdf form, accessible in the program documentation..

A more complicated shaft is the one from the Schaublin milling machine, with 3 NC axes, BT40 tool holder and a rotation speed of 9,000 rpm fig. 4.23–4.24. The same main shaft was modeled in SolidWorks Premium 2012 (fig. 4.24) to estimate errors in the calculation of eigenfrequencies using the proposed method. The errors were between 14.93% and 18.96% but in the same direction, having the character of a systematic error, clearly due to a coarser approximation specific to the proposed method.

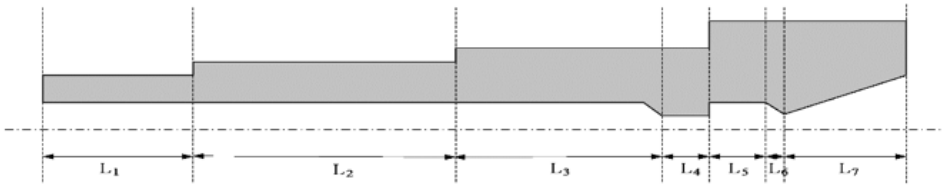

Fig. 4.23. Simplified main shaft model of the Schaublin machining center, with 3 numerically controlled axes, BT40 tool holder and maximum speed 9,000 rpm

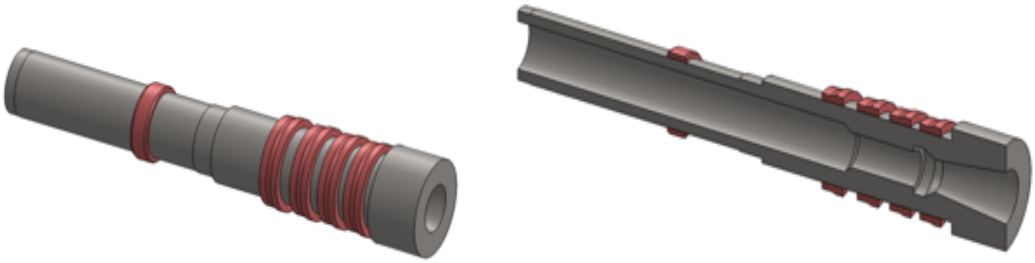

Fig. 4.24. SolidWorks 3D model of the main shaft assembly of Fig. 4.13

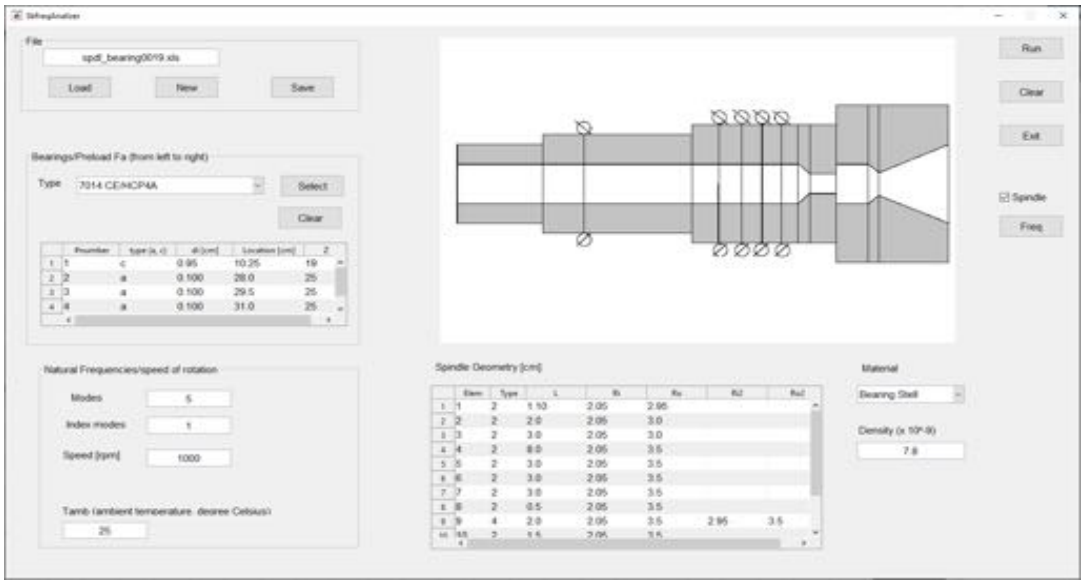

Fig. 4.25. GUI MATLAB module SbfreqAnalizer - Schaublin milling center, with 3 NC axes, BT40 tool holder

The main idea of practical use is to visualize the displacement of the frequencies as a function of speed in relation to the generation of heat in the bearings and the thermal deformation due to the change of the operating temperature of the main shaft. Screenshots from the software are shown in Figs. 4.25. To simplify the interface, when multiple values are transmitted, the defined separator is ";" (semicolon). The data reading module recognizes the terminators and extracts the values in the order in which they were entered. For example, the graph for frequencies 1 and 3 will be marked 1; 3, and the rotor speed "500; 1000; 1500; 2000; 3000; 4000; 5000; 6000 ".

4.4. CONCLUSIONS

Genetic algorithms are effective tools in optimization problems and, more recently, in solving nonlinear equations.

The difficulties encountered in the graphical user interface in the Matlab tool take more time to develop an automatic tool in the CAD tool style of an instrument in the MEF and multiphysics type (ANSYS, COMSOL). In section 4.4. a nonlinear approximation function based on an NN has been proposed, which describes a mathematical relationship given by the NN functionality between the eigenfrequencies and the speed / temperature vector of a real, simplified tree. The results are encouraging and in the future we will look for a simple enough analytical form to mathematically describe this relationship directly.

CHAPTER 5 COMPLEX THERMOMECHANICAL ANALYSIS OF EXTERNALLY DRIVEN MAIN SHAFTS - CASE STUDY

5.1. INTRODUCTION

In machine tool development or operation, research and design methods from the modeling and simulation category are used, such as Digital Block Simulation (DBS), finite element method (MEF) or systems simulation. Rigid Body Simulation (RBS) [36] separately or combined [64]. Each of the individual methods is limited in estimating the behavior of a main shaft assembly. Therefore, all these components must be assembled in such a way as to influence each other ([214], [213], [212], [196], [181], [177]). The thermodynamic method is a solution in some cases for analyzing the operation of bearings that is used by some authors ([151], [174]).

5.2. HEAT GENERATION IN BEARINGS

The usual dimensions of angular contact ball bearings used in the calculation are: r0 - outer diameter of the channel; r_i - the inner diameter of the channel; d_0 - diameter of the outer raceway; d_i - diameter of the inner raceway; D_0 - diameter of the ball; and Z - the number of balls. The model from fig. 5.1 and the geometry of 5.2 for solving which it is proposed to use a genetic algorithm with immigration operator

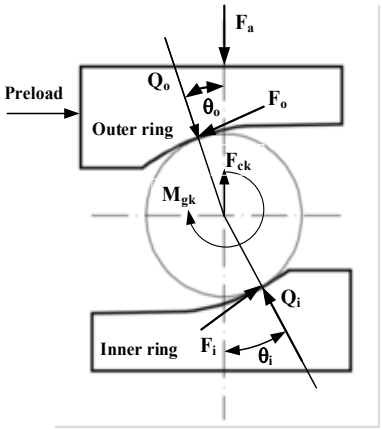

Fig. 5.1. Forces and moments in the ball-ring assembly

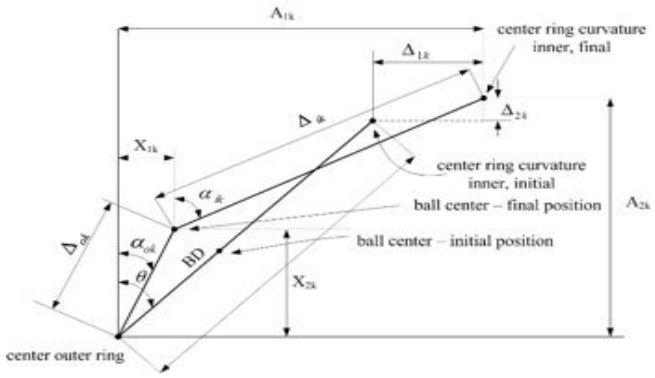

Fig. 5.2. Geometry in the operation of the ball-ring assembly

Hertz contact theory is used in order to model the contact force between the balls and the inner and outer ring (δ – ball's deformation).

$$(A_{1k} - X_{1k})^2 + (A_{2k} - X_{2k})^2 - \Delta_{ik}^2 = 0, \tag{5.1}$$

$$X_{1k}^2 + X_{2k}^2 - \Delta_{ok}^2 = 0, \tag{5.2}$$

$$Q_{ok}\cos\alpha_{ok} - \frac{M_{gk}}{D}\sin\alpha_{ok} - Q_{ik}\cos\alpha_{ik} + \frac{M_{gk}}{D}\sin\alpha_{ik} - F_{ck} = 0, \tag{5.3}$$

$$Q_{ok}\sin\alpha_{ok} + \frac{M_{gk}}{D}\cos\alpha_{ok} - Q_{ik}\sin\alpha_{ik} - \frac{M_{gk}}{D}\cos\alpha_{ik} = 0. \tag{5.4}$$

The interdependencies in equations (5.1) - (5.4) are related to the rotation frequency of the inner ring (or outer ring) fixed on the shaft and are given briefly by (the misalignment angle of the bearing is neglected) [79]:

$$\Delta_{ik} = (f_i - 0.5)D + \delta_{ik}, \tag{5.5}$$

$$\Delta_{ok} = (f_o - 0.5)D + \delta_{ok}, \tag{5.6}$$

$$A_{1k} = BD\sin\alpha^0 + \delta_a, \tag{5.7}$$

$$A_{2k} = BD\sin\alpha^0 + \delta_r\cos\psi_k, \tag{5.8}$$

$$\cos\alpha_{ok} = X_{2k}/[(f_0 – 0.5)D + \delta_{ok}], \tag{5.9}$$

$$\sin\alpha_{ok} = X_{1k}/[(f_0 – 0.5)D + \delta_{ok}], \tag{5.10}$$

$$\cos\alpha_{ik} = (A_{2k} - X_{2k})/[(f_0 – 0.5)D + \delta_{ik}], \tag{5.11}$$

$$\sin\alpha_{ik} = (A_{1k} - X_{1k})/[(f_0 – 0.5)D + \delta_{ik}], \tag{5.12}$$

$$F_{ck} = \frac{1}{2}mD\omega^2\left(\frac{\omega_E}{\omega}\right)_k^2, \tag{5.13}$$

$$M_{gk} = J\omega^2\left(\frac{\omega_\mathbf{b}}{\omega}\right)_k\left(\frac{\omega_E}{\omega}\right)_k\sin\alpha_k, \tag{15.4}$$

$$Q_{ik} = K_i \delta_{ik}^{3/2}, \quad Q_{ok} = K_o \delta_{ok}^{3/2}, \tag{5.15}$$

$$\alpha_k = \tan^{-1}(\sin\alpha_{ik} / (\cos\alpha_{ik} - h)), \tag{5.16}$$

$$\left(\frac{\omega_E}{\omega}\right)_k = \frac{\cos(\alpha_{ik} - \alpha_{ok}) - h \cdot \cos\alpha_{ok}}{1 + \cos(\alpha_{ik} - \alpha_{ok})}, \tag{5.17}$$

$$\left(\frac{\omega_B}{\omega}\right)_k = \frac{1}{h\cos\alpha_k} \cdot \frac{-1}{\left(\frac{\cos\alpha_{ok} + \tan\alpha_k \sin\alpha_{ok}}{1 + h\cos\alpha_{ok}} + \frac{\cos\alpha_{ik} + \tan\alpha_k \sin\alpha_{ik}}{1 - h\cos\alpha_{ik}}\right)}. \tag{5.18}$$

The *Newton-Raphson* numerical method is generally used to solve equations (5.1) - (5.4) and in this case the refinements proposed by [27] are used.

The heat generated by the rotation speed of the bearing n [rpm] is given by the additive relation of three friction torques: the load friction torque, the viscous friction torque and the spinning torque [79], [88], [103]. For the steel material and the number of Z-balls, the total heat generated by the angular contact bearing is given by (constant $1{,}047 \times 10^{-4}$ is specific for steel):

$$H_f = Z \cdot (1.047 \times 10^{-4} \cdot n \cdot M_t), \tag{5.19}$$

$$M_t = M_l + M_v + M_s, \tag{5.20}$$

where:

$$M_l = f_1 F_\beta d_m, \tag{5.21}$$

$$M_v = \begin{cases} 10^{-7} f_0 (\nu_0 n)^{2/3} d_m^3 & if\ \nu_0 n \geq 2000 \\ 160 \times 10^{-7} f_0 d_m^3 & if\ \nu_0 n < 2000 \end{cases}, \tag{5.22}$$

$$M_s = \frac{3\mu Q_i a_i E_i}{8}. \tag{5.23}$$

The notations are similar to those in [103]: d_m –pitch diameter, ν_0 – kinematic viscosity, n – shaft speed in rpm, f_0 – constant depending on the type of bearing and lubrication, (z, P_0, and C_0 are calculated based on tables), F_β – dynamic load, E_i – full second-order elliptic integral, a – the main axis of deformation of the ball shaped by an ellipse, and μ – friction coefficient.

The gyroscopic moment is taken into account for each ball of the bearing, even if it has a low value at high shaft speeds [79]:

$$M_g = \frac{1}{60} \cdot \rho \cdot \pi \cdot D^5 \cdot \omega_R \cdot \omega_M \cdot \sin\beta, \tag{5.24}$$

where ρ – material;'s density, ω_R – angular velocity of the ball around its own axis, ω_m – angular velocity of the ball, and β – the angle between the normal Z axis and the ball axis.

For cylindrical ball bearing in the equation (5.21) the spinning moment is zero, while F_l takes into account the contact line between the roller and the inner and outer raceways, so that depending on the friction the length of the cylinder L will be considered [32].

5.3. EXPERIMENTAL MEASUREMENTS ON THE MAIN SHAFT-BEARING BEARING ASSEMBLY

For the experimental tests, the main shaft-housing with bearings assembly was used, which belongs to a Shaublin type processing center and which was integrated in the experimental stand for thermomechanical analysis together with a set of temperature sensors, accelerometers, speed measuring transducer and a hardware-software block for the acquisition and processing of signals collected from sensors. Experimental measurements of dynamic and thermal behavior were performed directly on the machine tool after the main shaft had undergone major repair [64]. The experimental analysis aims to evaluate the dynamic and thermal parameters of the shaft. The measurement of shaft vibrations is performed by using accelerometers fixed on the front and rear of the main shaft (fig. 5.3). Thermal behavior is achieved by a non-contact Fluke laser sensor during axis rotation at a certain speed.

The measured values of temperature and vibration parameters are presented in tables 5.1, 5.2 and in fig. 5.4 - 5.5. The measurements show the vibration speeds of the main bearing L1 and the rear bearing L2 (fig. 5.6), as well as the level of acceleration to assess the condition of the bearings: front bearing - 0.51 g and rear bearing - 0.58 g (fig. 5.7). The frequency spectrum is shown in figs. 5.8.

Fig. 5.3. The transducers's psoition

Tabelul 5.1. Temperature monitoring

Speed *n* [rpm]	**Front bearing T_1 [°C]**	**Back bearing T_2 [°C]**	**Time [min]**
1000	29	30	18,00
1500	29	31	18,30
2000	30	31	19,00
2500	30	32	19,30
3000	32	33	19,50
3500	33	36	20,30
4000	30	33	20,47

Activated cooling			
4500	29	30	21,15
5000	29	30	21,30
5500	29	20	21,55
6000	29	30	22,20
6500	29	20	22,40
7000	29	31	22,51
7500	29	31	22,22
8000	29	31	23,50
8500	29	31	24.25

Tabelul 5.2. Vibration monitoring.

Speed *n* [rpm]	L_1 [mm/s]	*g*	L_2 [mm/s]	*g*
1006	0,07	0,15	0,04	0,18
2012	0,14	0,28	0,08	0,36
3018	0,15	0,64	0,09	0,78
4025	0,14	0,35	0,15	0,79
5031	0,31	0,29	0,23	0,83
6042	0,23	0,49	0,21	0,84
7043	0,41	0,63	0,42	1,07
8049	0,47	0,54	0,54	1,22
8553	0,52	0,62	0,64	1,31

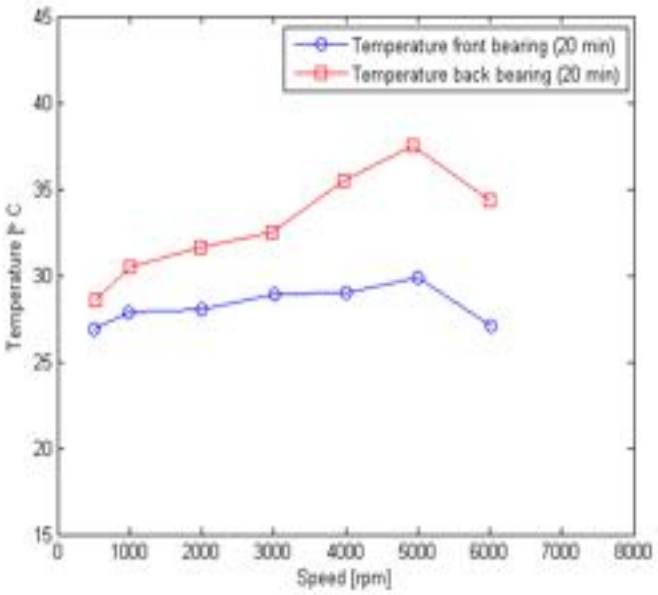

Fig. 5.4. Monitored temperature, for 6000 rpm (front bearing - T1max = 30 C, rear bearing - T2max = 36 C)

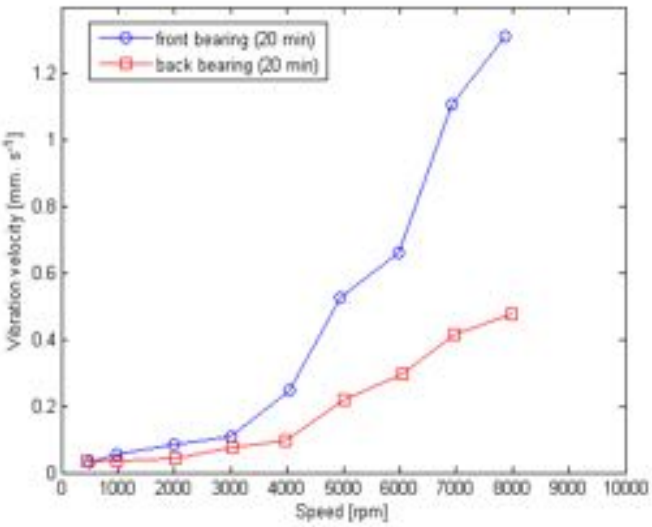

Fig. 5.5. Vibration speed

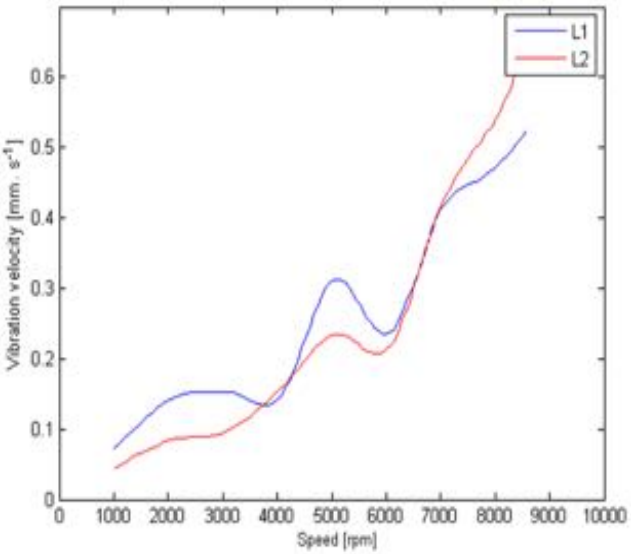

Fig. 5.6. Vibration speed depending on speed (L1, L2)

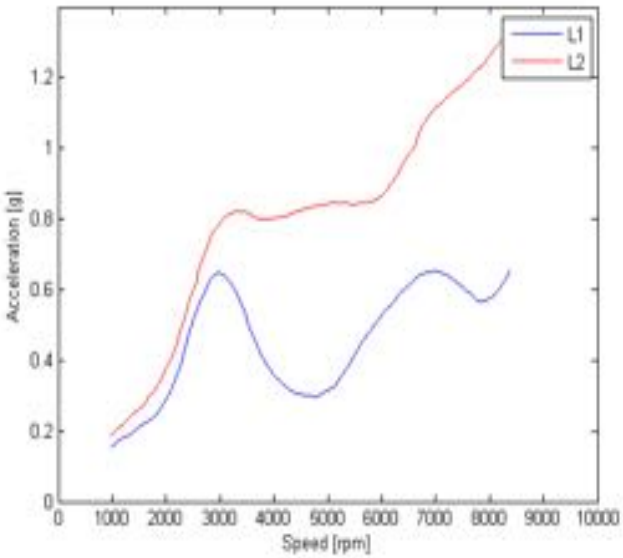

Fig. 5.7. Acceleration level depending on speed (L1, L2)

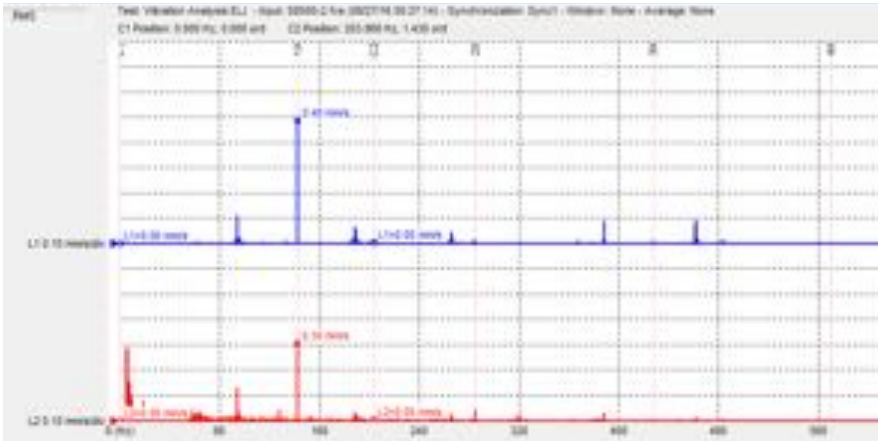

Fig. 5.8. Frequency spectrum at 8553 rpm

5.4. MODELING AND SIMULATION OF THE MAIN SHAFT SYSTEM

Two constructive variants were used for the main shaft [64]. The first was without cooling and therefore without a cooling circuit inside the housing (Fig. 5.9), and the second with a water cooling circuit. The simulations were performed on the whole having all the subcomponents, unlike most works in the field in which the simulations are performed on simplified versions of main shafts (without including bushings and sometimes spacers).

The main bearing shaft assembly consists of a quadruplex combination of two pairs of angular contact ball bearings mounted back to back, separated by spacers and a radial roller bearing at the rear. The bearings in the front bearing are pre-tensioned by the front nut and the rear bearing by the rear nut. The main shaft is driven by a Poly V belt wheel and the belt drive from an electric drive motor.

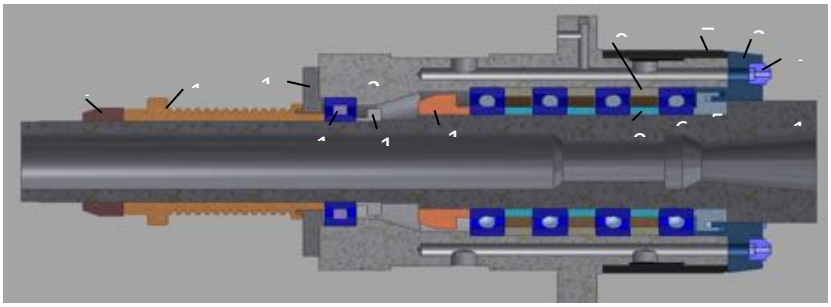

Fig. 5.9. Main shaft assembly without cooling (cross section)

Temperature distribution for the main shaft assembly without cooling is simulated at a maximum speed of 4,000 rpm after 120 minutes of running. It is measured at three points, in the same locations as in the experimental approach for assessing the accuracy of the model: 30° C in the front bearing location, 35° C in the rear bearing location and 33° C in the Poly V belt wheel area. the highest temperatures are in the area of the rear bearing (35° C), and in the area of the front bearing the temperature is 30° C on average. A higher load can be observed on the rear bearing, which takes over a higher reaction force caused by the tension of the belt tensioner. A uniformity of temperatures is observed on the geometric areas, the materials used having a better conductivity (Fig. 5.26 și 5.27).

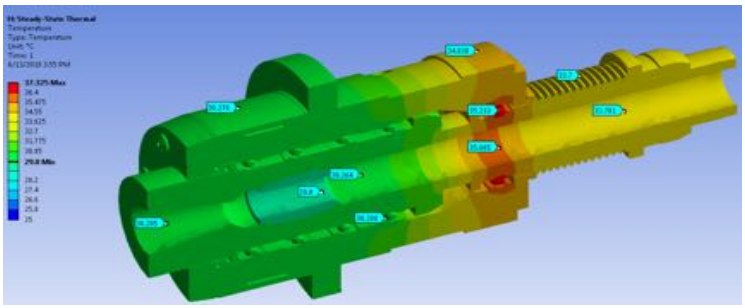

Fig. 5.26. Temperature distribution for the main shaft assembly without cooling and speeds up to 4,000 rpm

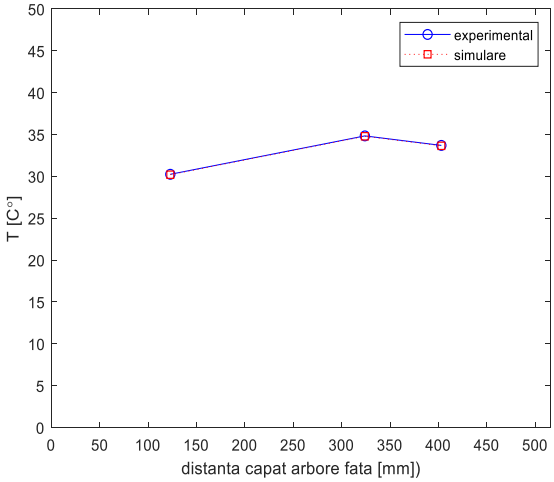

Fig. 5.27. Temperature distribution for the main shaft assembly without cooling (and speeds up to 4,000 rpm, experimental values and simulated values

The temperature distribution for the main coolant shaft assembly is simulated at a maximum speed of 8,500 rpm, starting at 4,500 rpm and gradually increasing for 180 minutes. The temperatures measured at the three points, both in experimental and simulation situations, are 29° C in the front bearing location, 30° C in the rear bearing location and 33° C in the area of the belt wheel. driven by a transmission through the Poly V belts (Fig. 5.28). Comparing the two situations, without cooling and with cooling, we can draw the following conclusions:

- In the first case, the shaft is heated more in the area of the rear bearing (35 ° C), but this area is reduced in size so as not to significantly influence its expansion. Thus, the heating is uniform, the temperature of the area for fixing the tool holder being 30° C.
- In the second case, even if the main shaft is cooled by the housing, the shaft temperature is higher but more evenly distributed. In the tool holder mounting area, the temperature is 33 ° C. The cooling system contributes to a more efficient cooling of the main shaft housing, which takes over most of the heat released by the bearings and the drive through the belts.

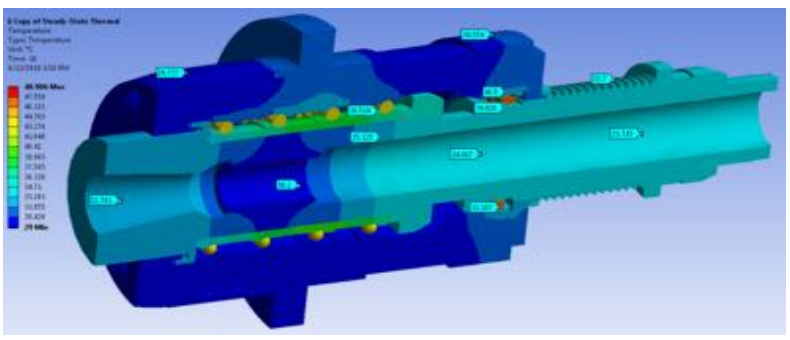

Fig. 5.28. Temperature distribution for the main shaft assembly with cooling system for speeds up to 8,500 rpm

The cooling system is very efficient, although it is geometrically complicated and creates some turbulence, as can be seen from the study of the coolant's flow (fig. 5.30). The main conclusions of the analysis of the behavior of the main shaft in the thermal field are:

- the need to resize the rear bearing of the main shaft, this being the main heating source;
- a new constructive solution must be used to release the rear end of the main shaft from the forces of the belt drive (discharged solution).

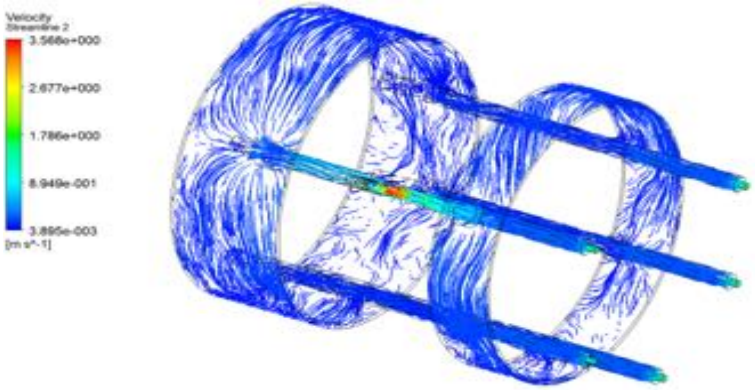

Fig. 5.30. Liquid circulation through the cooling system (speed distribution)

5.4.4 Transient Analysis

The transient analysis is performed under the same loading conditions as in the previous cases.

The results of these analyzes provide information about the deformations of the structures caused by the heat produced in the bearings and the transmission through the belts. The analysis is performed on the shaft without cooling (Fig. 5.31 și 5.32), as well as on the shaft with cooling (Fig. 5.33 și 5.34) operating at speeds up to 4,500 rpm. A predominantly axial displacement is observed, the maximum value of 11 μm being calculated in the rear area of the main shaft. As a result of these analyzes, it was found that the front bearing is sufficiently rigid and the thermal stresses do not induce deformations in this area (especially in the area of fixing the tool holder the deformations are below 1 μm). Even if the deformation values are higher, the accuracy of the shaft is not affected.

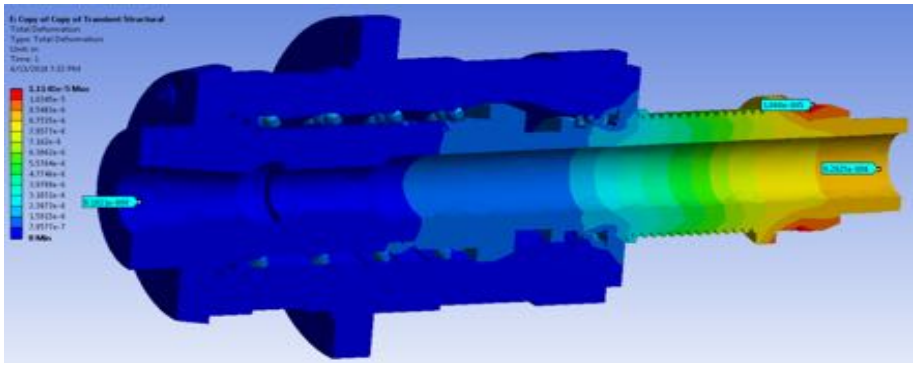

Fig. 5.31. Thermal deformations of the main shaft without cooling

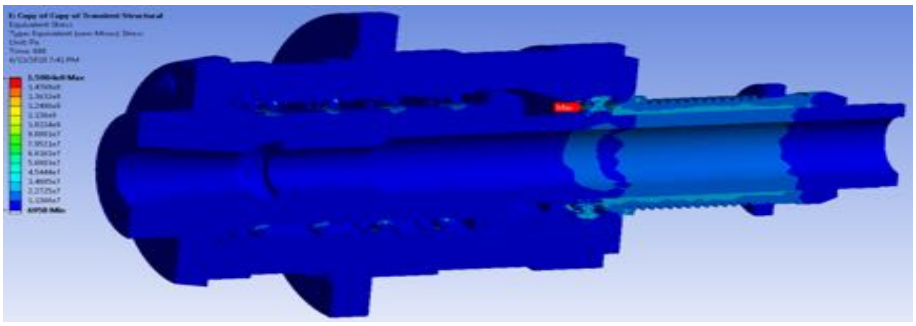

Fig. 5.32. Equivalent voltage distribution induced by thermal effects for the main shaft without cooling

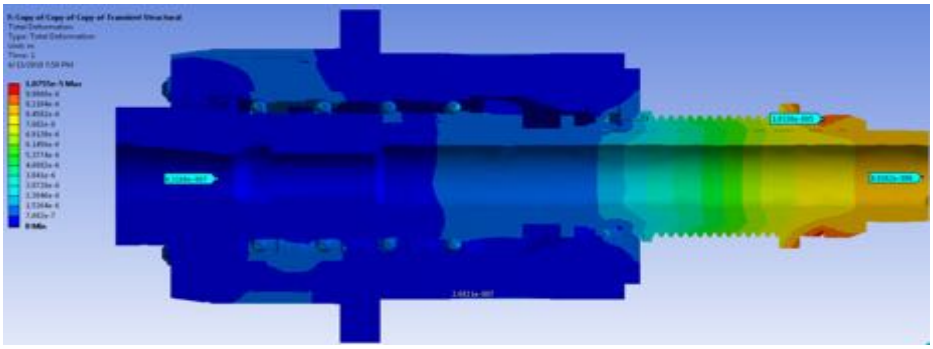

Fig. 5.33. Deformations of the main shaft under thermal effect with cooling

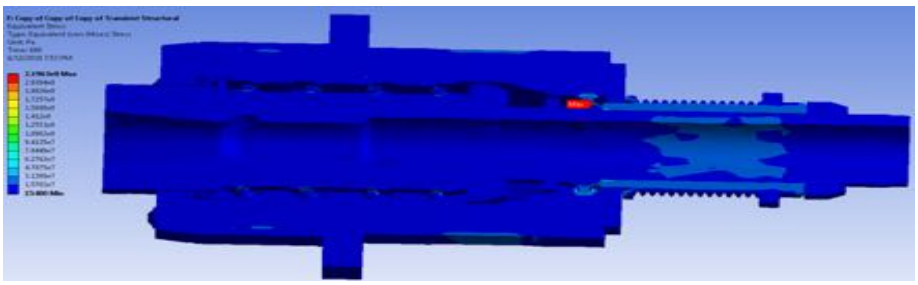

Fig. 5.34. Voltage distribution caused by thermal effect

Fig. 5.35. Eigenfrequencies of the main shaft assembly

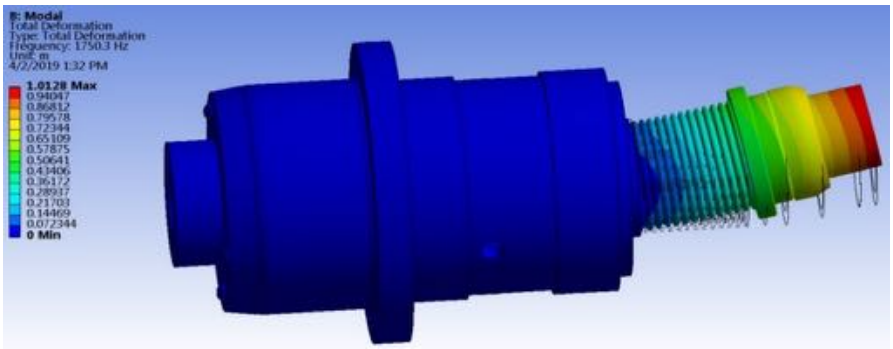

Fig. 5.36. Vibration mode 1

The stresses induced by the thermal effects are reduced, their maximum value (equivalent stress calculated according to the Von Misses criterion) being 159 MPa in the area of the rear bearing (Fig. 5.34). These values are lower than the allowable stresses of the materials used. Following the modal analysis, the eigenfrequencies of the main shaft system and the eigenmodes of vibrations are of interest (Fig. 5.35). It is observed that the first eigenfrequency has the value of f1 = 1750.3 Hz which is much higher than the rotation frequency for the maximum speed of 8500 RPM, which corresponds to the frequency fmax = 143.33 Hz. Figure 5.36 shows the vibration mode 1 of the main shaft assembly.

5.5. CONCLUSIONS

The paper had an approach to the level of CAD and thermomechanical FEA modeling of a main bearing-supported assembly [64]. The model corresponds to a real assembly that, in order to be validated, was subjected to experimental measurements. The mathematical modeling of the heat generated in the bearings is the basis of the thermal load of the FE model.

CHAPTER 6
CONCLUSIONS OF THE DOCTORAL THESIS, ORIGINAL CONTRIBUTIONS AND FUTURE RESEARCH DIRECTIONS

6.1. CONCLUSIONS OF THE DOCTORAL THESIS

The research on optimizing the functional behavior of shaft assemblies for high speeds was complex and laborious and involved an important original approach to the research. In fact this was to be expected given the complexity and difficulty of the topic and the motivation for and important premises for future research. Considering the research directions in this field, mechanical deformations, thermal analysis (including thermomechanical) and vibrations, the second topic was investigated, as an important novelty, the possible connections between the two. These connections, of an obviously complex nature, also required the application of unconventional mathematical techniques and methods, neural networks and genetic algorithms.

Thermomechanical analysis can be done classically, with FEM software tools (SolidWoks in the case studied) which may involve combined temperature-fluid cooling studies or on simplified models with scientific calculation software, MATLAB / Simulink in our case. It is noteworthy that, typically, the heat sources involved in the model (Q - amount of heat) are calculated separately and entered as a constant value in the EMF simulation. Although there are limited tests as an application, the amount of heat generated by angular contact ball bearings but also that generated by cylindrical roller bearings due to friction is a laborious process, with many variables to consider and more or less simplifying physical phenomena (e.g. gyroscopic moment).

For shafts with electric motor included, the generation of heat by the motor can be the determining factor of heat generation in copper windings. The general model of thermal calculation is based on the model of energy losses, which involves a very good knowledge of electrical and magnetic phenomena in AC motors. In addition, the problem of motor cooling through duct circuits depends on the fluid, duct geometry, pressure and flow rate provided by the coolant pump.

For all the studied cases it was considered that the working environment has an ambient temperature of 25ºC (in other cases the temperature is mentioned 25.5ºC) in accordance with the literature to have qualitative and quantitative terms of comparison in terms of the results of personal contributions.

A thermal stabilization of the assembly was found, between 10 minutes and 30 minutes, depending on the shaft's speed and working mode for the shaft with belt drive, Schaublin milling machining center, with 3 numerically controlled axes, BT40 tool holder and DELTA electric brush 4.5 OMLAT. Given these transition times, we consider that the analysis of this regime is also useful for the possible prediction of the time necessary to stabilize the thermal regime.

Almost all the works and studies in the field have as objective the thermomechanical analysis and the equations that give the angles α and αo, in some forms that are based on the same concept and that have a lot of circular dependencies. As a result, the convergence of solutions in numerical methods, generally based on the Newon-Raphson method, depends on the initial solution, which in this case must be quite close to the final solution, but also on the evolution of the Jacobian. As the variations from the static case can be very large, the viable solution is to fragment the space of combinations of the two angles for i in the interval $[0,2\pi]$. As a result, other alternatives, possibly based on evolutionary algorithms, may be a partially better solution in avoiding these problems.

Preloading in bearing assemblies plays an important role in generating heat in bearings by influencing ball bearing contact angles and, as a result, an optimization of their durability is strictly related to this variable. The theoretical results obtained in this thesis are consistent with data from the literature. The upload is predefined and must not exceed the manufacturer's catalog recommendations. Given the application considered, in other words, the geometry and the assembly shaft-bearings-housing being given, practically the only variables that can be modified in optimization according to a certain criterion (for example durability) are only preload and speed but also in a certain range of variation depending on the milled material, the cutting tool and the cutting parameters.

The temperature produced by cylindrical roller bearings was also taken into account, the calculation being much simpler, without preload forces. It was found that the value of heat generated by this type of bearings is significantly lower than that produced by ball bearings with similar dimensions of the inner and outer ring, but still at high speeds can produce amounts of heat of the order of 5–21 W.

Thermal networks are a viable and functional alternative for the thermomechanical analysis of the shaft. In addition, the use of the MATLAB environment allows the development of an integrated analysis for angular contact bearings such as: calculation of α_i and α_o angles $\rightarrow$ heat generated by the bearing $\rightarrow$ thermal network $\rightarrow$ results in various forms (graphics, tables, files). The big problem that remains to be solved in the future is the automatic discretization on the geometry of the shaft, housing, bearings, spacers and bushings for a complete analysis.

Neural networks have proven to be a good solution for approximating a model that describes a mathematical relationship given by NN functionality between natural frequencies and the rotational speed/temperature vector of a real, simplified shaft. The results are encouraging and in the future we will look for a simple enough analytical form to mathematically describe this relationship directly using physical phenomena and genetic programming.

The theoretical data obtained by modeling and simulation showed a good concordance compared to the experimental data and where it was not possible to obtain the experimental data, they were compared with those in the literature.

6.2. ORIGINAL CONTRIBUTIONS

The original contributions in this thesis, published, in the process of being published or in preparation for publication, are briefly as follows:

1. A complex analysis of the distribution of preload in a group of angular contact bearings, in possibly unbalanced distributions, arranged in tandem, m to the left and n to the right, section 3.1 of the thesis.
2. Analysis of heat phenomena in high speed shafts, with bearings and transmission of movement through the belt, section 3.2 of the thesis [58].
3. Analysis of heat phenomena in high speed shafts driven from the outside and the variant with AC electric motor (alternating current) included, theoretical approach and confirmation of research by experimental data, section 3.2 of the thesis.
4. Calculation of thermal deformations at the level of the shaft-bearing assembly with a predefined geometry with possible implications on the operation of the shaft in nominal parameters, section 3.3 of the thesis.
5. Bearing shaft models have been proposed using thermal networks with different degrees of complexity [60].
6. Application of evolutionary algorithms for complex problems in which solutions are difficult to find, such as the calculation of the contact angle for angular contact ball bearings, an essential variable for the calculation of the heat generated by the bearing [59].
7. Proposals for improved techniques for generating the thermal network that models the transmission of heat through bearing shafts, techniques that use thermal networks [60].
8. Analysis of temperature-frequency dependence for a bearing shaft [62].
9. A complex thermomechanical analysis of externally driven main shafts. Finite element modeling and simulation using CAD and multiphase software (SolidWorks). The simulation data were compared with the experimental data. It was considered the case of shafts with cooling and without cooling. The published findings are the subject of future research to improve the reliability of the shaft and bearings [62].
10. Transient thermomechanical analysis of externally driven main shafts [62].
11. Optimizing the reliability of angular contact ball bearings according to the working parameters of the shaft section 3.5 of the thesis.
12. Possible applications of dynamic shaft models with bearings in medicine [17]**.**
13. Use of a neural network as a predictor for the relationship between temperature, speed and natural frequency of the shaft assembly [62].
14. Development of graphical GUI interfaces in MATLAB for an interactive and user-friendly view for the relationship between temperature, shaft speed and natural frequency, a premise for future contribution to software dedicated to the dynamics of the bearing shaft, as a toolbox for MATLAB [62].
15. Genetic algorithm and model for multicriteria optimization of constructive dimensions (bearing positions, main diameters, clamping force) based on a multiple objective function having as variable parameters its own frequencies and the maximum temperature in points considered at the carcass surface.

All the theoretical and practical objectives of the doctoral thesis have been achieved and the premises for further research have been created for future research for several objectives

whose results can be based on those validated by the doctoral thesis. They will be able to bring other novelty results in the future.

6.3. FUTURE RESEARCH DIRECTIONS

Based on the results of personal contributions from the doctoral thesis and on research in progress, we can make a summary of future research:

1. software designed as a toolbox for the complex thermomechanical analysis of the main shafts driven from the outside with automatic discretization of the geometry in 2D symmetrical section and interactive graphic correction. The model uses the semi-automatic construction of thermal networks that include the housing of the assembly;

2. Identify a mathematical relationship between speed, temperature generated in bearings, geometry factors and eigenfrequencies in shafts without cooling and transmission of external motion using genetic programming algorithms;

3. Optimization of the reliability of the shaft and bearings in dynamic mode, for a predefined curve of speeds, preload and forces in the cutting process. The use of genetic algorithms for optimization goal functions has proven to be a viable method that will be used in future research;

4. In the future, the optimal working regime of the cooling shaft will also be analyzed, taking into account an analysis of the variables that influence an objective function such as the reliability of the main shaft assembly.

BIBLIOGRAPHY

[1] *M. L. Adams*, Rotating Machinery Vibration: From Analysis to Troubleshooting, CRC Press, 2000.

[10] *B. Bediz, B. Arda Gozen*, *E. Korkmaz*, *O. Burak Ozdoganlar*, Dynamics of ultra-high-speed (UHS) spindles used for micromachining, International Journal of Machine Tools and Manufacture, **vol. 87**, pp. 27–38, 2014.

[12] *T. L.* Bergman, Adrienne S. Lavine, Frank P. Incropera, David P. DeWitt, Fundamentals of Heat and Mass Transfer, 7th Edition, Wiley, 2011.

[15] *A. Boglietti*, *P. Ferraris*, *M. Lazzari*, Power Derating for Inverter Fed Induction Motors, Proceedings of the 29th IAS Annual Meeting (IEEE), **vol. 1**, pp. 55–61, 1994.

[17] *D. Bonneau, A. Fatu, D. Souchet*, Hydrodynamic Bearings, Wiley-ISTE, 2014.

[18] B. Bossmanns, Thermomechanical modeling of motorized spindle systems for high-speed milling, PhD Thesis, Purdue University, 1997.

[19] *B. Bossmanns, Jay F. Tu*, A thermal model for high speed motorized spindles, International Journal of Machine Tools & Manufacture, **vol. 39**, no. 9, pp. 1345–1366, 1999.

[20] *B. Bossmanns, J.F. Tu*, A power flow model for high speed motorized spindles – heat generation characterization, J. Manuf. Sci. Eng., **vol. 123**, no. 3, 2000, pp. 494–505.

[21] *B. Bossmanns, J.F. Tu*, A power flow model for high speed motorized spindles–heat generation characterization, ASME Journal of Manufacturing Science and Engineering, **vol. 123**. no. 3, pp. 494–505, 2001.

[22] *E.R. Bowen , J.O. Medwell*, A thermohydrodynamic analysis of journal bearings operating under turbulent conditions, Wear, **vol. 51**, issue 2, pp. 345–353, 1978.

[23] *C. Brecher, Y. Shneor, S. Neus, K. Bakarinow, M. Fey*, Thermal Behavior of Externally Driven Spindle: Experimental Study and Modelling, Engineering, **vol.** 7, pp. 73–92, 2015.

[24] *D. Brewe, B. Hamrock*, Simplified Solution for Elliptical-Contact Deformation Between Two Elastic Solids, ME Trans., J. Lub. Tech., **vol. 101**, no. 2, pp. 231–239, 1977.

[25] *W. Brian Rowe*, Principles of Modern Grinding Technology, Elsevier, 2014.

[26] Van-Canh Tong, Jooho Hwang, Jongyoup Shim, Jeong-Seok Oh, Seong-Wook Hong, Multi-objective Optimization of Machine Tool Spindle-Bearing System, International Journal of Precision Engineering and Manufacturing, **vol. 21**, pp. 1885–1902, 2020.

[27] *Y. Cao, Y. Altintas*, A General Method for the Modeling of Spindle-Bearing Systems, Journal of Mechanical Design, **vol. 126**, 2004, pp. 1089–1108.

[28] *Y. Cao*, Modeling of High-Speed Machine-Tool Spindle Systems, PhD thesis, The University of British Columbia, 2006.

[32] *H. Cao, T. Kang, X. Chen*, Noise analysis and sources identification in machine tool spindles, CIRP Journal of Manufacturing Science and Technology, **vol. 25**, pp. 26–35, May 2019.

[33] *Y.A. Cengel, A.J. Ghajar*, Heat and Mass Transfer: Fundamentals and Applications, McGraw Hill Education, 5th Edition, 2014.

[36] *G. Constantin*, Capitol: Virtual în concepția și exploatarea de mașini-unelte și sisteme de mașini, în Modelare-Simulare-Proiectare în domeniul mașinilor-unelte și sistemelor de mașini, Ed. G. Constantin, Editura Printech, București, pp. 9–79, 2014.

[40] *R. Dupont*, Robust rotor dynamics for high-speed air bearing spindles, Precision Engineering, **vol. 40**, pp. 7–13, 2015.

[41] *R.H. Engelmann, W.H. Middendorf*, Handbook of Electric Motors, Marcel Dekker, 1995.

[47] *D. Fedorynenko, R. Kirigaya, Y. Nakao*, Dynamic characteristics of spindle with water-lubricated hydrostatic bearings for ultra-precision machine tools, Precision Engineering, **vol. 63**, pp. 187–196, May 2020.

[50] *M.I. Friswell, J.E.T. Penny, S.D. Garvey, A.W. Lees*, Dynamics of Rotating Machines, Cambridge University Press, 2010.

[54] *G. Genta*, Vibration of Structures and Machines, Springer-Verlag New York, 1995.

[55] G. Genta, Dynamics of Rotating Systems, Springer-Verlag New York, 2005.

[58] ***A. Gheorghita***, D. Arotaritei, M. Turnea, G. Constantin, Modelling and simulation of high seed spindle, current problems and optimizations – a survey, Proceedings in Manufacturing Systems, **vol. 11**, issue 1, pp. 215–222, 2016 (ProQuest, IndexCopernicus).

[59] ***A. Gheorghita****, M. Turnea, M. Rotariu, G. Constantin, D. Arotaritei*, A New Proposal for Solving Equations of Angular Contact Ball Bearing Using Evolutionary Techniques, 6th International Conference on Advancements of Medicine and Health Care through Technology; 17–20 October 2018, Cluj-Napoca, Romania, pp. 241–245 WOS:000493501100037.

[60] ***A. Gheorghita****, D. Arotaritei, G. Constantin, M. Turnea, M. Ilea, M. Rotariu*, Thermal model of externally driven spindle: a semi-automatic construction of thermal network, Proceedings in Manufacturing Systems, **vol 13**, Issue 1, pp. 21–26, 2018 (ProQuest, IndexCopernicus).

[61] ***A. Gheorghita****, D. Arotaritei, G. Constantin*, E-Learning Tutorial for Contact Angle Ball Bearings in Dynamic Models with Applications in Medicine, The 14th International Scientific Conference eLearning and Software for Education Bucharest, vol. 3, pp. 395–402, 2018, WOS:000467471000059.

[62] ***A. Gheorghita****, G. Constantin, D. Arotaritei*, Analysis of temperature dependent natural frequencies of spindles with possible application in medicine, The 16th International Scientific Conference eLearning and Software for Education Bucharest, April 23–24, 2020 (EBSCO).

[63] *M. Ghinea*, Cercetări teoretice şi experimentale privind utilizarea ceramicii tehnice în construcţia de maşini-unelte, Teză de doctorat, Universitatea Politehnica din Bucureşti, 1999.

[64] *G. Constantin, C. Dogariu, C.F. Bîşu,* ***A. Gheorghiță****, D. Arotăriței, I. G. Ghionea*, Complex thermo-mechanical analysis of externally driven main spindles – a case study, Acta Technica Napocensis, Series: Applied Mathematics, Mechanics, and Engineering, **vol 63**, nr. 1, pp. 27–38, 2020, WOS:000528235300004.

[68] *A.O. Gibson, J. L. Stein, J.F. Tu*, A Thermomechanical Model of High-Spindle Bearing Systems for use in the Design of Spindle Bearing Load Control Systems, ASME Journal of Basic Engineering June, 1960, 309-3.

[69] *D.E. Goldberg*, Genetic Algorithms in Search, Optimization, and Machine Learning. Addison-Wesley Professional, 1996.

[79] *T.A. Harris*, Rolling Bearing Analysis, 4th Edition, Wiley-Interscience, 2001,

[81] *T.A. Harris, M.N. Kotzalas*, Advanced Concepts of Bearing Technology, Taylor & Francis, 5th Edition, 2006.

[82] Harris, T.A. An Analytical Method to Predict Skidding in High Speed Roller Bearings. ASLE Trans., **vol. 9**, pp. 229–24, 1996.

[84] S. Haykin, Neural Networks – A Comprehensive Foundation, Prentice Hall, 1998.

[88] *T. Holkup, H. Cao, P. Kolár, Y. Altintas, J. Zelený*, J, Thermo–mechanical model of spindles, Ann. Manuf. Technol., **vol. 59**, no. 1, pp. 365–368, 2010.

[90] *H. Li, Y.C. Shin*, Integrated Dynamic Thermo-Mechanical Modeling of High Speed Spindles, Part 1: Model Development, Journal of Manufacturing Science and Engineering, **vol. 126**, no. 1, pp. 148–157, 2004.

[103] *C. Jin, B.W. Y. Hu*, Heat generation modeling of ball bearing based on internal load distribution, Tribology International, **vol. 45**, pp. 8–15, 2012.

[104] *A. Jones*, Analysis of Stresses and Deflections, New Departure Engineering Data, Bristol, Conn. 1946.

[106] *H.E. Jordan*, Energy-Efficient Electric Motors and Their Applications, 2nd Edition, Springer Science+Business Media New York, 1994.

[107] *B.R. Jorgensen, Y.C. Shin*, Dynamics of Machine Tool Spindle/Bearing Systems Under Thermal Growth, Journal of Tribology, **vol. 119**, pp. 875–882, 1997.

[109] *A. Jula, M. Lateş*, Organe de maşini, Editura Universitatii Transilvania, Brasov, 2004.

[110] *T. R. Kane, D. A. Levinson*. Dynamics: Theory and Applications, McGraw-Hill, New York, 1985.

[114] *S.M. Kim, S.K. Lee*, Prediction of Thermo-Elastic Behavior in a Spindle-Bearing System Considering Bearing Surroundings, International Journal of Machine Tools and Manufacture, **vol. 41**, no. 6, pp. 809–831, 2001.

[116] *S.M. Kim, S.K. Lee*, Spindle Housing Design Parameter Optimization Considering Thermo-Elastic Behaviour, Int J. Adv Manuf Technol. **vol. 5**, pp. 1061–1070, 2005.

[118] *J.D. Kim, I. Zverv, K.B. Lee*, Thermal Model of High-Speed Spindle Units, Intelligent Information Management, **vol. 2**, pp. 306–315, 2010.

[124] Junning Li, Jiafan Xue, Zhitao Ma, Study on the Thermal Distribution Characteristics of High-Speed and Light-Load Rolling Bearing Considering Skidding, Appl. Sci. 2018.

[136] *D.L. Logan*, A First Course in the Finite Element Method, 5th Edition, CL Engineering, 2011.
[138] *C.V. Madhusudana*, Thermal contact conductance, Switzerland, Springer, 2014.
[139] *D.M. Marin*, Studii teoretice şi cercetări experimentale privind comportarea statică şi dinamică a arborelui principal de la centrele de prelucrare prin frezare, Teză de doctorat, Universitatea Politehnica din Bucureşti, 2009.
[148] *K. Nakajima*, Thermal contact resistance between balls and rings of a bearing under axial, radial, and combined loads, J. Thermophys. Heat Transf., **vol. 9**, pp. 88–95,1995.
[151] *A. Nica*, A thermohydrodynamic method of bearing analysis, Tribology, **vol. 4**, issue 4, pp. 218–226, 1971.
[155] *B.A. O'Leary*, Analysis of high-speed rotating systems using Timoshenko beam theory in conjunction with the transfer matrix method, MSc. Thesis, Rochester Institute of Technology, 1989.
[161] *F. Pouly, C. Changenet, F. Ville*, Power loss predictions in high-speed rolling element bearings using thermal networks, Tribol Trans, 53, pp. 957–967, 2010
[163] *N. Predincea,* Studiul deformaţiilor termice şi elastice ale maşinilor-unelte şi al influenţei acestora asupra parametrilor de performanţă, Teza de doctorat, Institutul Politehnic din Bucuresti, 1991.
[166] *M. Rades*, Dinamica Masinilor, Editura Printech, 2008.
[167] J.*S. Rao*, Rotor Dynamics, Third edition, New Age International, 1996.
[168] *J.S. Rao*, History of Rotating Machinery Dynamics, Springer, Dordrecht, 2011.
[174] *J. M. Sansinenea, R. M. Bueno*, Computer aided design of standardized hydrostatic journal bearings, Proceedings of the Fifteenth International Machine Tool Design and Research Conference, pp 175–183, 1975.
[177] *X. Min, J. Shuyun, C. Ying*, An improved thermal model for machine tool bearings. Int J Mach Tool Manuf , **vol. 47**, pp. 53–62, 2007.
[180] *D.A. Stephenson, J.S. Agapiou*, Metal Cutting Theory and Practice, Third Edition, CRC Press, 2016.
[181] *F. Tan, L. Wang, M. Yin, G. Yin*, Obtaining more accurate convective heat transfer coefficients in thermal analysis of spindle using surrogate assisted differential evolution method, Applied Thermal Engineering, **vol. 149**, pp. 1335–1344, 2019.
[182] *J. Takabi, M.M. Khonsari*, On the thermally-induced failure of rolling element bearings, Tribology International, **vol. 9**4, pp. 661–674, 2016.
[183] *V.T. Than, J.H. Huang*, Nonlinear thermal effects on high-speed spindle bearings subjected to preload, Tribology International, **vol. 96**, pp. 361–372, 2016.
[185] *R. Tiwari*, Rotor systems: analysis and identification, CRC Press, 2017.
[189] *E. Udup*, Contribuţii privind optimizarea transferului de căldură în ansamblurile mecanice de tip arbore – lagăre cu rulmenţi prin analiză termodinamică, Teză de doctorat, Universitatea Politehnica din Bucureşti, 2013.
[191] *A. Vintilescu*, Cercetări teoretice şi experimentale privind diagnosticarea prin vibraţii a ansamblului arbore principal-lagăre pentru maşini-unelte, Teză de doctorat, Universitatea Politehnica din Bucureşti, 2012.
[192] *D.C. Vişan*, Modelarea Dinamică a Sistemelor Rotor-Lagăre, Editura PRINTECH, 2008.
[196] *L. Xiaohu, Y. Lv, K. Yan, J. Liu, J. Hong*, Study on the influence of thermal characteristics of rolling bearings and spindle resulted in condition of improper assembly, Applied Thermal Engineering, **vol. 1145**, pp. 221–233, March 2017.
[207] *A. Zivkovic, M. Zeljkovic, S. Tabakovic, Z. Milojevic*, Mathematical modeling and experimental testing of high-speed spindle behavior, Int. J. Adv. Manuf. Technol., **vol. 77**, pp. 1071–1086, 2015.
[211] *J. Zhang, B. Fang, J. Hong, S. Wan, Y. Zhu*, A general model for preload calculation and stiffness analysis for combined angular contact ball bearings, Journal of Sound and Vibration, **vol. 41122**, pp. 435–449, December 2017.
[212] *Y. Zhang, X. Li, J. Hong, K. Yan, S. Li*, Uneven heat generation and thermal performance of spindle bearings, Tribology International, **vol. 126**, pp. 324–335, October 2018.
[213] *Y. Zhang, T. Liu, W. Gao, Y. Tian, X. Qi, P. Wang, D. Zhang*, Active coolant strategy for thermal balance control of motorized spindle unit, Applied Thermal Engineering, **vol. 134**, pp. 460–468, 2018.
[214] *D. Zheng, W. Chen*, Thermal performances on angular contact ball bearing of high-speed spindle considering structural constraints under oil-air lubrication, Tribology International 109, pp. 593–601, 2017.